DEVELOPMENTAL BIOLOGY

ERK phosphorylates chromosomal axis component HORMA domain protein HTP-1 to regulate oocyte numbers

Debabrata Das, Shin-Yu Chen, Swathi Arur*

Oocyte numbers, a critical determinant of female reproductive fitness, are highly regulated, yet the mechanisms underlying this regulation remain largely undefined. In the *Caenorhabditis elegans* gonad, RAS/extracellular signal–regulated kinase (ERK) signaling regulates oocyte numbers; mechanisms are unknown. We show that the RAS/ERK pathway phosphorylates meiotic chromosome axis protein HTP-1 at serine-325 to control chromosome dynamics and regulate oocyte number. Phosphorylated HTP-1(S325) accumulates in vivo in an ERK-dependent manner in early-mid pachytene stage germ cells and is necessary for synaptonemal complex extension and/or maintenance. Lack of HTP-1 phosphorylation leads to asynapsis and persistence of meiotic double-strand breaks, causing delayed meiotic progression and reduced oocyte number. In contrast, early onset of ERK activation causes precocious meiotic progression, resulting in increased oocyte number, which is reversed by removal of HTP-1 phosphorylation. The RAS/ERK/HTP-1 signaling cascade thus functions to monitor formation and maintenance of synapsis for timely resolution of double-strand breaks, oocyte production, and reproductive fitness.

INTRODUCTION

Oocyte number in metazoans is an indicator of ovarian reserve and a measure of reproductive success, whereby higher oocyte number correlates with increased reproductive fitness (*1*, *2*). Regulation of oocyte number therefore is critical for female fertility. In mammals, female germline stem cells are finite in number and are depleted before the female is born (*3*). Thus, oocyte number is thought to be largely regulated through apoptosis (*3*). During fetal development, female germ cells undergo differentiation through meiosis I to form oocytes, which makes it technically challenging to study these processes in a mammalian model.

Meiosis I is governed by a series of evolutionarily conserved events of chromosome behaviors during the first prophase stage. These include homologous chromosome (homolog) pairing, formation, and maintenance of a meiosis-specific structure known as the synaptonemal complex (SC), programmed DNA double-strand break (DSB) formation, crossover formation, and chromosome remodeling (*4*–*7*). A measure of successful meiosis is often defined by the ability of oocytes to generate euploid embryos (*4*, *8*, *9*). Delay in any of the meiotic events leads to defects in chromosome segregation, which, in turn, cause infertility in the mother or aneuploidy in the progeny (*8*, *9*). Errors in meiosis also activate checkpoint mechanisms that reduce the oocyte number through apoptosis (*10*). However, the consequences of speeding up the events of meiosis I in any system remain unknown, and thus, mechanisms that govern the rate of meiotic progression remain undefined. What also remains unknown is the nature of the timer, which might control meiotic progression itself and its physiological importance, if any.

Caenorhabditis elegans oogenesis occurs continuously in the adult gonad, rendering it a genetically tractable system to investigate these questions (*4*). Similar to mammals, *C. elegans* oogenesis is controlled by the conserved receptor tyrosine kinase/RAS/extracellular signal–regulated kinase (ERK) signaling pathway (*11*–*14*). Complete lack of ERK activation in the granulosa cells in mammals results in lack of germinal vesicle breakdown and meiotic arrest (*14*); lack of ERK activation in worms causes meiotic arrest in mid-pachytene (*11*, *15*). Sustained ERK activation for ~12 hours in mammalian oocytes, from prometaphase of meiosis I until the end of meiosis II, is essential for many steps of meiotic progression (*12*). In *C. elegans*, sustained (~18 hours) ERK activation in the mid-pachytene stage of meiosis I is essential for progression of meiosis I (*11*, *16*). For example, reduction in ERK signaling results in extension of the mid-pachytene stage—a phenotype known as "pachytene progression"—increased apoptosis and lower oocyte numbers (*11*, *16*, *17*). Intriguingly, gain-of-function in ERK signaling in *C. elegans* causes a dramatic increase in oocyte numbers, albeit of low quality (*11*, *16*). These observations reveal that the RAS/ERK signaling pathway functions as a rheostat to regulate oocyte number and thus quality. However, the cellular and molecular mechanisms through which RAS/ERK signaling regulates oocyte numbers remain unknown.

Common mechanisms that regulate cell numbers downstream to the RAS signaling pathway in any developmental context involve regulation of proliferation and apoptosis (*18*–*20*). Investigating the role of either proliferation or apoptosis in regulation of RAS-mediated control of oocyte numbers in this study revealed that the RAS/ERK pathway does not regulate either apoptosis or proliferation to control oocyte number. Instead, we show that ERK phosphorylates HTP (HIM-3 paralog)–1, a HORMA (HOP1, REV7, and MAD2) domain-containing protein and one of the chromosome axis components during meiosis I at serine-325 in vitro and in vivo. Phosphorylation of HTP-1(S325) is necessary for SC extension and/or maintenance. Lack of HTP-1(S325) phosphorylation results in asynapsis of the chromosomes and persistence of meiotic DSBs [as assayed by RAD (radiation sensitivity abnormal)–51 foci], causing delayed meiotic progression and reduced oocyte number; we also observe asynapsis in the ERK loss-of-function mutant animals. Increased and ectopic ERK activation in the RAS gain-of-function mutants results in precocious meiotic progression, resulting in increased oocyte number, which is reversed upon removal of HTP-1 phosphorylation.

Department of Genetics, UT MD Anderson Cancer Center, Houston, TX 77030, USA.
*Corresponding author. Email: sarur@mdanderson.org

Restoring HTP-1 phosphorylation in the ERK loss-of-function mutants rescues the reduced oocyte number, through correction of the SC defects. Together, our data suggest that ERK activation provides the signaling threshold in early-mid pachytene to coordinate SC formation and/or maintenance, via HTP-1 phosphorylation, with meiotic progression to result in the formation of healthy oocytes and progeny.

RESULTS

RAS/ERK signaling regulates oocyte number independent of proliferation and apoptosis

In the *C. elegans* hermaphroditic germ line, stem cells are housed in the progenitor zone (PZ) and proliferate throughout the adult reproductive life of the animal (Fig. 1A). The progenitor cells enter meiosis I in the transition zone (TZ) and proceed through a long meiotic prophase I to form a linear row of oocytes resulting in a spatiotemporally organized tissue (Fig. 1A). ERK is activated in two zones in oogenic germ cells in wild-type animals, zone 1 in mid-pachytene and zone 2 in arrested diakinesis oocytes (Fig. 1, A and B). An increase in RAS/ERK signaling [as assayed through a temperature-sensitive gain-of-function mutation L19F in the guanosine triphosphatase domain of RAS/LET (Lethal)–60 (*21*); *let-60(ga89 gf)*, called *RAS(act)* in this study] causes a sharp increase in oocyte number, with the gonad displaying nearly double the number of oocytes of 26.84 ± 6.84 relative to 13.64 ± 3.15 oocytes per gonad arm in wild-type animals at the restrictive temperature of 25°C (Fig. 1, C and D). Reduction of RAS/ERK signaling [as assayed through a temperature-sensitive loss-of-function mutation in the mitogen-activated protein kinase kinase (MPK) binding domain in ERK/MPK-1 (*22*); *mpk-1(ga111 rf)*, called *ERK(loss)* in this study] leads to a corresponding decrease in oocyte number (9.98 ± 3.6) relative to wild-type animals at 25°C (Fig. 1, C and D). In both the backgrounds (at the restrictive temperature of 25°C), the oocytes formed are of low quality, and the mutant animals are either sterile or produce progeny that do not survive past early larval stages of development (*11*). At the permissive temperature of 20°C, the *RAS(act)* and *ERK(loss)* mutants display oocyte numbers and quality similar to wild-type animals (fig. S1, A and B).

To determine the mechanisms through which RAS/ERK signaling regulates oocyte number, we investigated proliferation and apoptosis, which regulate cell numbers in most organ systems (*23*–*25*). In the wild-type *C. elegans* germ line, the progenitor germ cells proliferate in the PZ region to populate and grow the germ line, and the meiotic germ cells undergo apoptosis in the late-pachytene region (Fig. 1A). We investigated the PZ cell pool and mitotic index in the RAS/ERK mutants and the effect of blocking progenitor cell proliferation on oocyte number in *RAS(act)* animals. Assessment of total number of PZ cells and mitotic index (Materials and Methods and fig. S2, A to C) revealed no difference in proliferation in the two mutant backgrounds at any temperature or condition tested, relative to wild type (fig. S2, D to G). These data suggest that the rate of proliferation does not correlate with oocyte number in the RAS/ERK signaling mutants. Next, we blocked proliferation in *RAS(act)* and wild-type animals at both 20° and 25°C using hydroxyurea (HU), which inhibits DNA synthesis (Materials and Methods) (*26*). The HU treatment led to a complete block in germline PZ proliferation, which resulted in an overall reduction in total germ cell numbers in wild-type and *RAS(act)* germ lines (fig. S3, A and B). However, the block in proliferation did not affect the increased number of oocytes in *RAS(act)* mutants (Fig. 1E and fig. S3, C to F). These data demonstrate that proliferation does not regulate activated RAS-dependent increase in oocyte numbers.

To investigate the role of apoptosis in regulating oocyte number, we assessed apoptotic germ cell numbers in both *RAS(act)* and *ERK(loss)* mutants using live imaging to visualize engulfed cell corpses encircled by the scavenger receptor CED-1::GFP driven by the *lim-7* promoter in gonadal sheath cells (*27*, *28*) (Materials and Methods and fig. S4A). Both the *RAS(act)* and *ERK(loss)* mutants displayed increased ($P = 0.030$ and $P = 0.032$, respectively) cell death relative to wild-type animals at 25°C (Fig. 1F), but not at 20°C (fig. S4B), suggesting that apoptosis is not correlated with oocyte number in this context. The increase in apoptosis in *ERK(loss)* and *RAS(act)* mutant germ lines is consistent with previous observations (*17*, *29*). Nevertheless, we genetically blocked apoptosis in the *ERK(loss)* mutants to investigate whether blocking apoptosis could rescue the lower oocyte number. CED-3/Caspase is required for apoptosis; *ced-3(n717)* null mutants do not exhibit germ cell apoptosis and display oocyte numbers similar to wild type (Fig. 1G and fig. S4, C and D) (*30*). *ERK(loss);ced-3(n717)* double-mutant germ lines are indistinguishable from *ERK(loss)* single-mutant germ lines with respect to low oocyte numbers at 25°C (Fig. 1G and fig. S4, E to H), suggesting that blocking cell death does not rescue the low oocyte number in animals with loss of ERK signaling. Together, we conclude that apoptosis does not regulate ERK-dependent loss of oocyte number.

RAS/ERK signaling regulates meiosis I progression to maintain oocyte numbers

The results obtained for proliferation and apoptosis (above) were unexpected and led us to query the similarities and differences in the pattern of ERK activation in *RAS(act)* mutant germ lines at 20° or 25°C, since oocyte numbers are affected at 25°C, but not 20°C. *RAS(act)* germ lines at 20° and 25°C display continuous activation of ERK in the loop region (Fig. 2, A and B), which, while distinct from the ERK activation pattern in wild type (Fig. 1B), does not correlate with the specific increase in oocyte number in *RAS(act)* at 25°C. Notably, *RAS(act)* germ lines display early onset of ERK activation at 25°C relative to 20°C in the mid-pachytene region (Fig. 2, A to C), leading to the hypothesis that the early onset of ERK activation in mid pachytene of *RAS(act)* germ lines at 25°C drives precocious exit of germ cells from pachytene to commence oocyte formation at diplotene stage, in turn leading to increased oocyte number.

To test whether germ cells are spatially exiting pachytene precociously in *RAS(act)* germ lines at 25°C, we used the length of PZ, TZ, and pachytene regions as a measure of germ cell progression via analysis of germ cell rows using chromosomal morphology and GLD (germ line development)–1 accumulation as markers for the germ cell stage (Materials and Methods) (*31*); GLD-1 accumulation falls at the "loop" region where pachytene cells transit to diplotene stage oocytes in wild-type germ lines (Fig. 2, D and E, and fig. S5, A to H). *RAS(act)* germ lines display significantly lower number of pachytene germ cell rows relative to wild-type germ lines at 25°C (25.33 ± 2.31 and 36.04 ± 1.68, respectively) in these analyses (Fig. 2, D and E, and fig. S5, C to G). These observations suggest that the *RAS(act)* germ cells precociously exit pachytene to form diplotene stage oocytes. In contrast, *ERK(loss)* mutant at 25°C leads to delayed

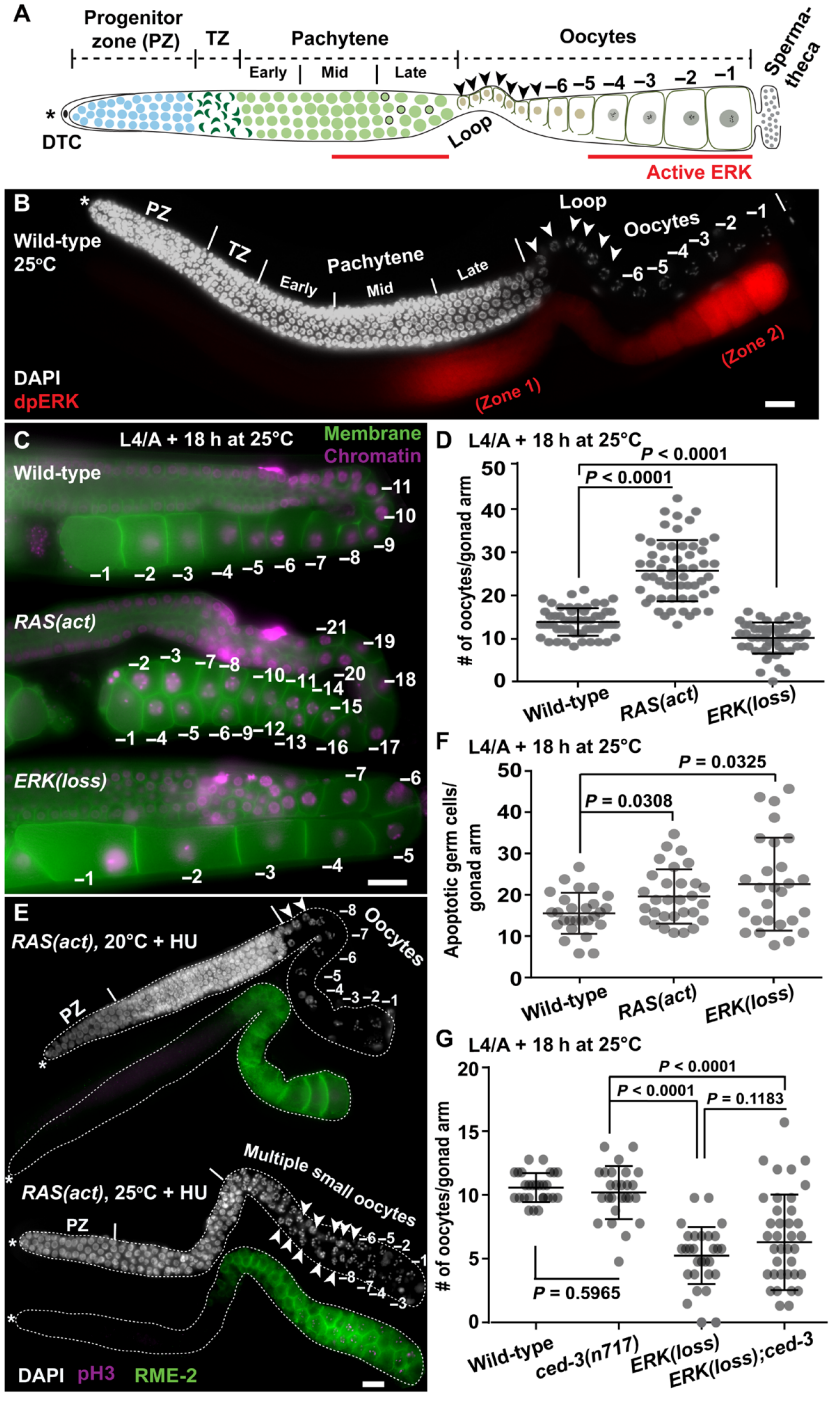

Fig. 1. Proliferation and apoptosis do not affect RAS/ERK signaling-mediated control of oocyte numbers. (**A**) Schematic surface view of a hermaphroditic *C. elegans* germ line displaying the spatiotemporal nature of germ cell organization with a distal (*) to proximal orientation from left to right. Proliferative PZ cells are in the distal region, capped by the distal tip cell (DTC). Germ cells enter meiosis in the TZ, followed by progression through different stages of meiosis I. Germ cells undergo apoptosis (black circles) in the late-pachytene stage. At the loop region, diplotene stage germ cells start to form oocytes and undergo meiotic arrest in diakinesis. The loop region forms the anatomic bend in the gonad. (**B**) Representative dissected wild-type germ lines immunostained with anti–di-phosphorylated (dp) ERK (active ERK, in red) and DNA [4′,6-diamidino-2-phenylindole (DAPI), white]. (**C**) Representative live-fluorescent images of wild-type, *RAS(act)*, and *ERK(loss)* mutants displaying germline morphology marked by pH domain membrane green fluorescent protein (GFP; green) and histone H2B::mCherry (magenta). −1 marks the proximal end and oldest oocyte. (**D**) Scatter dot plot of oocyte numbers from the indicated genotypes. (**E**) Representative dissected germ lines from HU-treated *RAS(act)* animals immunostained with DAPI (DNA, white), anti–p-histone H3 (to mark dividing cells, magenta), and anti–RME-2 (to mark oocytes, green) at indicated temperature. (**F**) Quantification of apoptotic germ cells from indicated genotypes. (**G**) Quantification of oocyte numbers from indicated genotypes. Each experiment was repeated three times, $n = 30$ to 60 per genotype. Statistical significance was calculated by a nonparametric Mann-Whitney test, and scatter dot plots are represented as means ± SD. *P* values are noted between groups compared. Arrowhead indicates an oocyte. Scale bars, 25 μm.

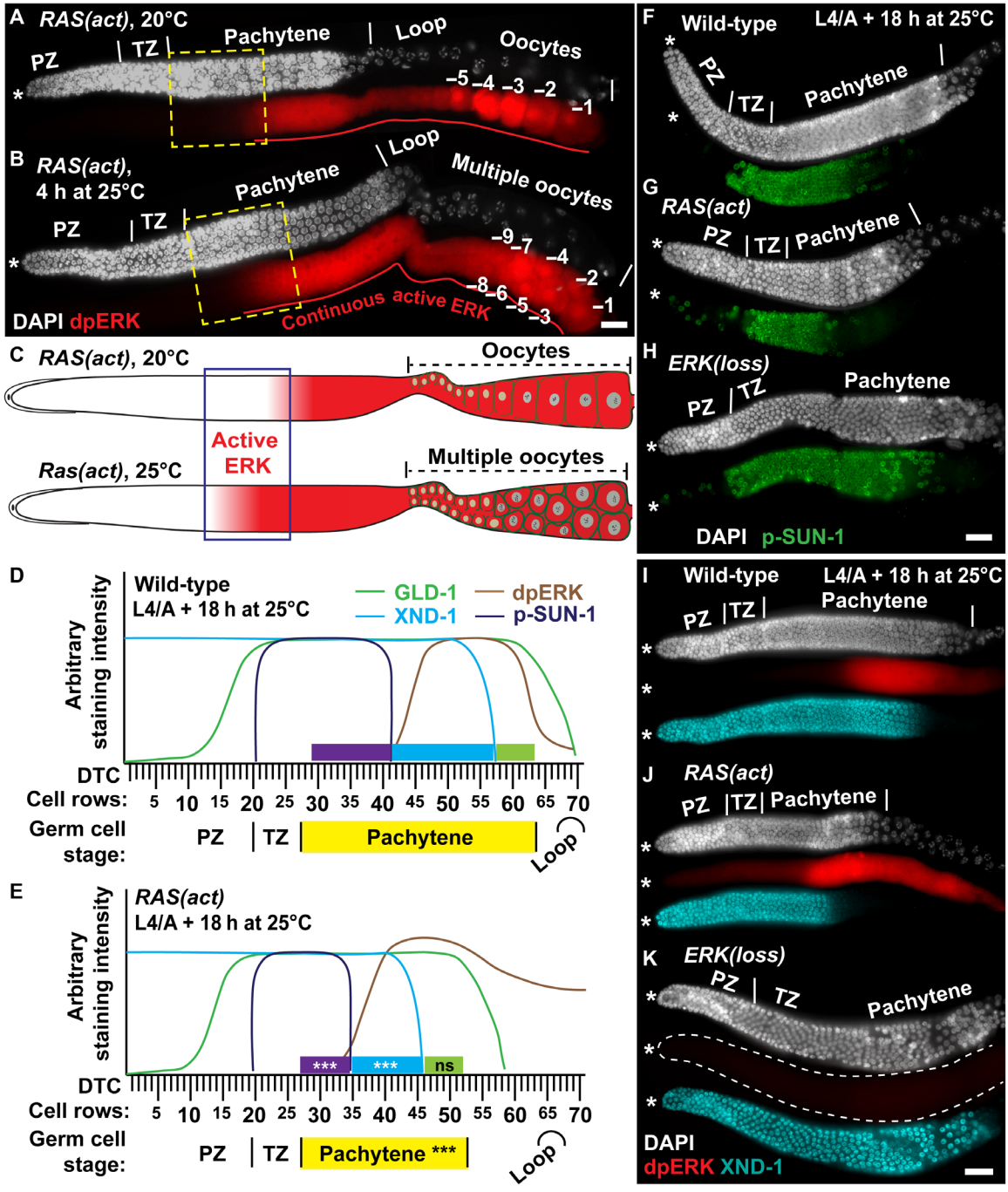

Fig. 2. RAS/ERK signaling regulates early- and mid-pachytene meiotic progression. Germ lines are displayed with DTC on the left (asterisks) of the photograph. (**A** and **B**) Representative images of dissected *RAS(act)* germ lines probed with anti-dpERK (red) and DAPI (DNA, white). Yellow dashed box highlights the region of early onset of ERK activation at 25°C in *RAS(act)* germ lines. (**C**) Schematic representation of *RAS(act)* germ line displaying the early onset of active ERK in pachytene region and the multiple oocyte phenotype at 25°C. (**D** and **E**) Graphical representation displaying the accumulation pattern of various markers assayed in the study. The *y* axis represents arbitrary staining intensity. The *x* axis displays the positional value of a germ cell and its corresponding meiotic stage. The graphs are generated with the mean values from the data shown in fig. S5. Purple bar represents p-SUN-1–positive cell rows sans TZ. Cyan bar represents XND-1–positive cell rows sans p-SUN-1–positive cell rows. Green bar represents XND-1–negative pachytene germ cell rows. *** indicates significant difference; ns, not significant, based on fig. S5. (**F** to **H**) p-SUN-1(S8) (green) localization and DAPI (DNA, white) in dissected germ lines of indicated genotypes. (**I** to **K**) Localization of dpERK (red), XND-1 (cyan), and DAPI (DNA, white) in the indicated genotypes. Scale bar, 25 μm.

exit of pachytene stage germ cells, persistent GLD-1 accumulation, and fewer number of oocytes (fig. S5H). These data together suggest that activation of RAS/ERK signaling in pachytene regulates oocyte numbers likely through regulation of meiotic progression.

To determine whether early onset of ERK activation in *RAS(act)* germ lines at 25°C drives the early exit of pachytene cells into diplotene, we assayed for meiotic progression at TZ and early-mid pachytene boundary using p-SUN-1(S8) (*32*) and at mid-late pachytene boundary using XND (x-chromosome nondisjunction factor)–1 (*33*). p-SUN-1(S8) and XND-1 are meiotic regulators that accumulate in distinct regions of the germ line along the distal-proximal axis, and their dynamics mirrors the stage of meiotic germ cells. p-SUN-1(S8) accumulates from TZ until mid pachytene in wild type, while XND-1 accumulates until late pachytene in wild-type germ lines. Currently, there are no established markers to assay meiotic progression of early-mid pachytene transition. However, molecules like p-SUN-1(S8) persist in accumulation in germ cells if there is any defect in early stages of meiosis, including pairing, synapsis, or meiotic DSBs (*32*), and can thus be used as a marker for meiotic progression. Using these markers, we tested the hypothesis that early onset of ERK activation in the early-mid pachytene region of *RAS(act)* germ lines results in an increased rate of pachytene progression leading to shorter early-mid pachytene boundary in the *RAS(act)* mutant germ lines. As hypothesized, we observed that p-SUN-1(S8) and XND-1 accumulation falls spatially earlier in *RAS(act)* germ lines in pachytene relative to wild type at 25°C (Fig. 2, D to J, and fig. S5, I and J). Graphically superimposing these data for both p-SUN-1(S8) and XND-1 reveals that the mid-pachytene region, characterized by XND-1–positive and p-SUN-1(S8)–negative cells is shorter in the *RAS(act)* germ lines at 25°C. Late-pachytene stage germ cell rows as assessed by loss of XND-1 staining are similar in *RAS(act)* and wild-type germ lines at 25°C (Fig. 2, D and E, and fig. S5K), suggesting that late pachytene is not affected by an increase in RAS signaling. In contrast to *RAS(act)* mutant germ lines, the *ERK(loss)* germ lines display persistence of p-SUN-1(S8)– and XND-1–positive cell rows at 25°C relative to wild type (Fig. 2, H to K), consistent with the model that RAS/ERK signaling regulates the rate of meiotic progression in the early- and mid-pachytene regions. Together, these data suggest that germ cells are transitioning from early to mid pachytene precociously in the *RAS(act)* mutant and that this progression controls oocyte number.

RAS-mediated increase in oocyte numbers is suppressed by loss of SC formation

If the rate of meiotic progression through early and mid pachytene is the limiting factor for regulating oocyte number, then we reasoned that slowing down meiotic progression in *RAS(act)* mutants should decrease the oocyte number and suppress the *RAS(act)* mutant phenotype. Early- and mid-pachytene are characterized by SC formation and maintenance and meiotic DSB accumulation for crossover formation. These two processes are uncoupled in *C. elegans* (*34*), unlike in yeast or mice where DSB formation is required for homolog pairing and occurs before SC assembly (*5*). Thus, using RNA interference (RNAi) analysis, we tested whether slowing down the rate of meiotic progression through perturbation of either of these two processes regulates oocyte number. SC in *C. elegans* is composed of six central region proteins [SYP (synapsis in meiosis abnormal)–1, SYP-2, SYP-3, SYP-4, SYP-5, and SYP-6] and four axial element proteins [HIM (high incidence of males)–3, HTP-1, HTP-2 and HTP-3] (*4*). To destabilize the SC, we depleted *him-3*, which is essential for SC formation (*35*). To interfere with DSB formation, we depleted *spo-11*, a type IV topoisomerase, essential for DNA DSB formation (*34*). We performed *him-3* and *spo-11* RNAi in wild-type and *RAS(act)* background together with *luciferase* RNAi as a control (Fig. 3, A to F). We confirmed the RNAi efficiency via assaying for univalent chromosomes in diakinesis oocytes (Fig. 3G), which are formed because of loss or improper chromosome remodeling upon loss of SC or DSB function (*4*). Notably, *him-3* RNAi led to a suppression of the increased oocyte phenotype in the *RAS(act)* germ lines at 25°C (Fig. 3, A to F). *him-3* RNAi also leads to a significant reduction in oocyte number in wild-type germ lines relative to *luciferase* RNAi controls (Fig. 3H and fig. S6A). *spo-11* RNAi had no impact on oocyte number in either wild-type (Fig. 3, A to C) or *RAS(act)* (Fig. 3, D to F) mutants at either 20° or 25°C (Fig. 3H and fig. S6A). These data suggest that disrupting SC formation in the wild-type and *RAS(act)* germ lines affects oocyte numbers, likely through an effect on meiotic progression.

To test whether *him-3* RNAi altered the rate of meiotic progression, we assayed *him-3* RNAi and control RNAi germ lines for p-SUN-1(S8) accumulation. Analysis of p-SUN-1(S8) accumulation in *him-3* and control RNAi revealed a significant ($P < 0.0001$) expansion of p-SUN-1(S8)–positive cell rows in *RAS(act)* and wild-type germ lines treated with *him-3* RNAi relative to control (*luciferase*) RNAi (Fig. 3, I to K, and fig. S6, B and C). These data suggest that early meiotic progression is delayed upon *him-3* RNAi, likely resulting in the suppression of oocyte numbers in *RAS(act)* germ lines. Thus, we hypothesize that RAS/ERK signaling regulates the rate of meiosis I progression and oocyte numbers by regulating SC formation in *C. elegans*.

HTP-1 is an in vitro and in vivo substrate of ERK

SYP-2 is an ERK substrate in worms and regulates chromosome segregation (*36*) rather than meiotic progression. To identify the components of SC that intersect with ERK signaling in regulating SC formation and oocyte numbers, we performed an in silico search for ERK phosphoacceptor sites [as described in (*17*)] on the axial and central element components of the SC. We identified HIM-3, HTP-1, HTP-2, HTP-3, SYP-1, SYP-2, and SYP-4, but not SYP-3, SYP-5, or SYP-6, as putative ERK substrates through this approach. We then performed ERK2 in vitro kinase assays on recombinant full-length purified proteins of each of the putative axial and central element proteins as described (Fig. 4, A and B) (*17*). We identified two previously unidentified in vitro ERK2 substrates—the HORMA domain containing axial element proteins HTP-1 and HTP-3 (Fig. 4B). In our hands, SYP-2 was not phosphorylated in this assay (Fig. 4B); thus, we focused on HTP-1. A recent study showed that HTP-1 is phosphorylated on the N-terminal region, downstream to Polo-like kinase 1 (PLK-1) and PLK-2 (*37*), whereas the putative ERK phosphoacceptor sites are C-terminal (Fig. 4C). Using site-directed mutagenesis, we converted each potential ERK2 phosphoacceptor site on HTP-1 to alanine (alanine substitution of serine renders the protein unphosphorylatable) (Fig. 4D). These assays identified HTP-1 serine-325 as an ERK-dependent phosphoacceptor in vitro (Fig. 4E).

To determine whether HTP-1(S325) is phosphorylated in vivo and to investigate its spatial and cellular localization, we generated a phospho-specific antibody against the seven–amino acid peptide [AQMS*PIQ] surrounding HTP-1(S325) [Materials and Methods

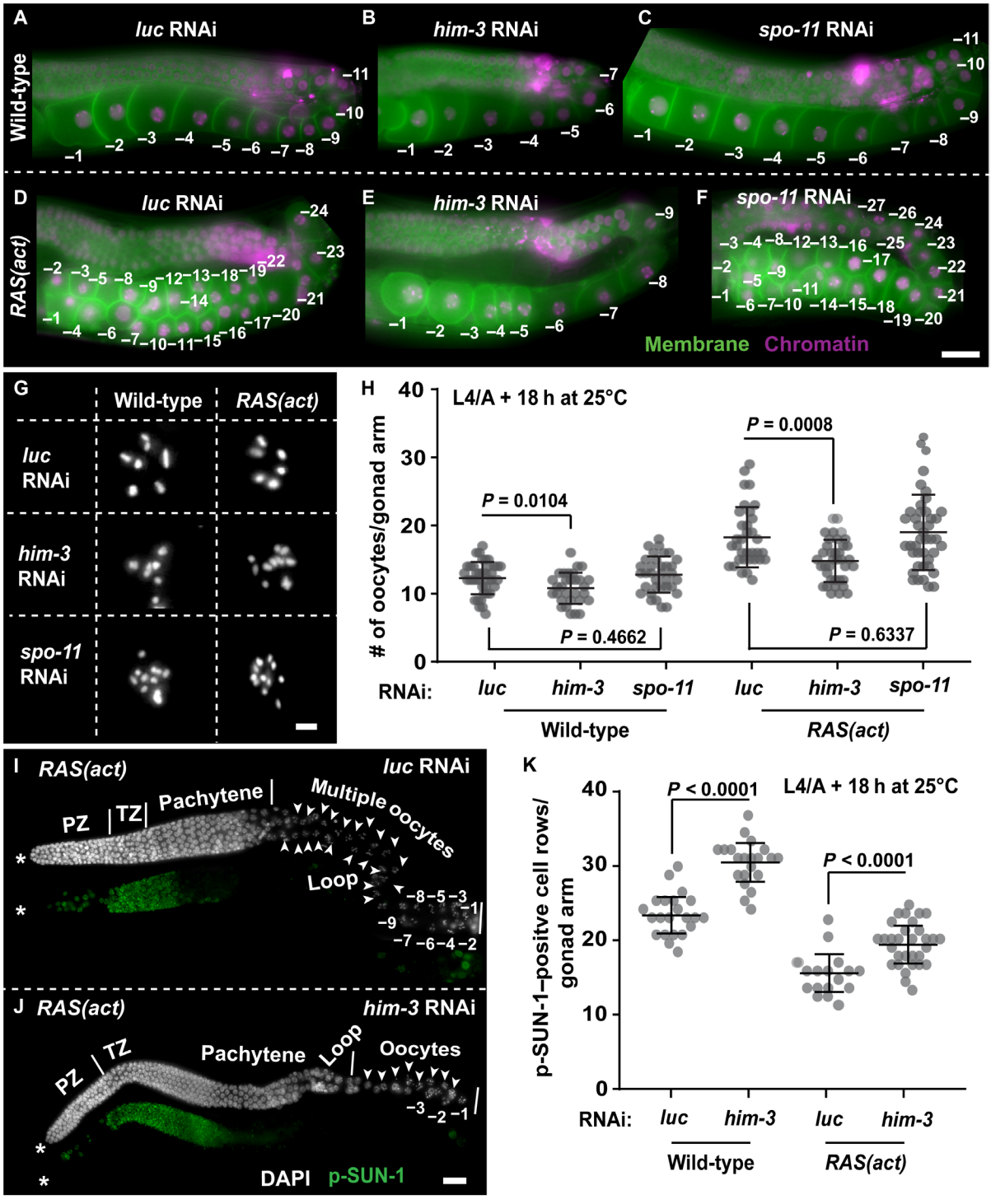

Fig. 3. *him-3* RNAi suppresses the increased oocyte numbers in *RAS(act)* animals. (**A** to **F**) Representative live-fluorescent images of wild-type and *RAS(act)* mutants displaying oocytes (marked with membrane-tagged GFP in green) and chromatin (histone H2B tagged in red) upon control (*luciferase*), *him-3*, and *spo-11* RNAi. Images are oriented with the loop on the right side in the photograph and oocytes on the ventral end of the animal. Oocytes are numbered from proximal to distal polarity (toward loop). The most proximal oocyte is labeled as −1. (**G**) Representative photograph of DAPI-stained (white) diakinesis chromosomes of −1 oocyte from indicated RNAi treatment groups. *him-3* and *spo-11* RNAi oocytes display univalent chromosomes. (**H**) Scatter dot plot with quantification of oocyte number in the indicated genotypes upon control (*luciferase*), *him-3*, and *spo-11* RNAi treatment. (**I** and **J**). Representative *RAS(act)* dissected germ lines upon control (*luciferase*) and *him-3* RNAi labeled with p-SUN-1(S8) (green) and DAPI (DNA, white). Germ lines are oriented with the DTC on the left of the photographs (asterisks). (**K**) Quantification of DAPI (DNA, white) and p-SUN-1(S8) (green) germ cell rows from wild-type and *RAS(act)* mutants upon control (*luciferase*) and *him-3* RNAi. Experiments were repeated three times, $n = 25$ to 30 per genotype. Statistical significance was calculated by Mann-Whitney nonparametric test. Error bars represent means ± SD. Scale bars, 25 μm [for (A) to (F), (I), and (J)] and 5 μm [for (G)].

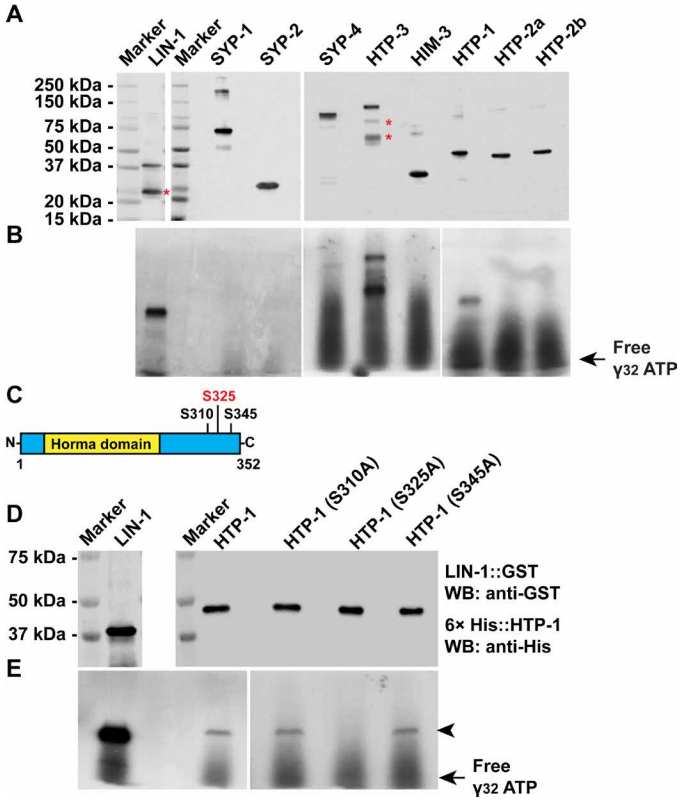

Fig. 4. Active ERK phosphorylates axial element proteins HTP-1(serine325) and HTP-3 in vitro. (**A**) Western blot analysis using anti-His antibody to visualize recombinant 6× His-tagged full-length central and axial element proteins of the SC. (**B**) Autoradiographs of in vitro ERK2 kinase assay of the central and axial element proteins from (A) demonstrates phospholabeling of HTP-1 and HTP-3 in vitro. ATP, adenosine triphosphate. (**C**) HTP-1 protein structure with putative (black) and confirmed (red) ERK phosphorylation sites. (**D**) Western blot (WB) analysis using anti-His antibody to visualize HTP-1 wild-type and serine to alanine edited proteins. (**E**) Autoradiographs of in vitro ERK2 kinase assays reveal serine-325 as the HTP-1 phosphoacceptor in vitro. LIN (abnormal cell lineage)–1 is the positive control for the in vitro ERK2 kinase assay. Red asterisks indicate degraded protein. The kinase assays for each protein were performed twice in an independent replication of the data.

(*17*, *38*)]. Phosphorylated HTP-1(S325) [p-HTP-1(S325)] accumulates in the TZ and pachytene and into diplotene stage oocytes in wild-type and *RAS(act)* germ lines (Fig. 5, A to C, and fig. S7). In TZ, p-HTP-1(S325) localizes to the nucleus and nucleoplasm and along the chromosomes. As germ cells progress into late pachytene, p-HTP-1(S325) staining concentrates along parts of the SC, as detected by coimmunostaining with SYP-1, while a majority of the signal is localized to the nucleoplasm (Fig. 5D). In diplotene stage oocytes, p-HTP-1(S325) accumulates in the nucleoplasm and chromatin and is colocalized with SYP-1 (Fig. 5E). In diakinesis oocytes, p-HTP-1(S325) staining is diffuse and drops in levels (Fig. 5F). The p-HTP-1(S325) accumulation pattern remains high in the loop region, likely because a phosphatase distinct from the dual-specificity ERK phosphatase (*39*) mediates its dephosphorylation. The anti–p-HTP-1(S325) signal is specific to HTP-1 phosphorylation at serine-325 and is not detected in either *htp-1(gk105)* deletion mutant or upon loss of HTP-1(S325) phosphorylation site (Fig. 5, G and H).

To determine whether p-HTP-1(S325) is dependent on ERK activation in vivo, we assayed the ERK(null) allele, *mpk-1(ga117)* mutant germ lines. *mpk-1(ga117)* germ cells arrest in the mid-pachytene stage (*15*). In more than 90% of the *mpk-1(ga117)* germ lines, we did not observe any accumulation of p-HTP-1(S325). However, in ~10% of the *mpk-1(ga117)* dissected germ lines, we observed a low-level accumulation of p-HTP-1(S325) (Fig. 5I), which suggests that a second kinase may redundantly phosphorylate HTP-1 in vivo, while the majority of HTP-1 phosphorylation may depend on ERK. To test whether this low level of HTP-1(S325) phosphorylation in *ERK(null)* germ lines is due to lower HTP-1 protein, we performed Western blot analysis using HTP-1/2 antibody. We find that the total level of HTP-1 is not affected by loss of ERK activation (Fig. 5J). These data together demonstrate that HTP-1 is phosphorylated at S325 in vivo in an ERK-dependent manner.

p-HTP-1(S325) regulates oocyte number downstream to RAS/ERK signaling

To determine the function of HTP-1(S325) phosphorylation on meiotic progression and oocyte number in vivo, we generated an unphosphorylatable HTP-1 [*htp-1(viz62)*, referred to as *HTP-1(S325A)* from here on] and a phosphomimetic HTP-1 [*htp-1(viz67)*, referred to as *HTP-1(S325E)* from here on] mutant alleles using CRISPR-Cas9 genome editing technology [Materials and Methods and Fig. 6A, (*40*)]. Phospho-editing of serine-325 of HTP-1 to either alanine or glutamic acid did not affect its protein stability as assessed by Western blot analysis (Fig. 6B) or accumulation of HTP-1/2 on the chromosomal axis (fig. S8). To assess whether lack of HTP-1 phosphorylation or constitutive HTP-1 phosphorylation affects meiosis I per se, we characterized the phosphomutant alleles for their germline morphology, brood size, embryonic lethality, and high incidence of male (Him) phenotype (Fig. 6, C to H). *HTP-1(S325A)* mutant germ lines exhibit univalent chromosomes in diakinesis nuclei, which is a hallmark of meiotic impairment. Relative to wild-type −1 to −4 diakinesis oocytes, which display 6 4′,6-diamidino-2-phenylindole (DAPI) bodies (indicative of six bivalent chromosomes), the *HTP-1(S325A)* mutant oocytes display 6 to 10 DAPI bodies with >70% of diakinesis oocytes displaying 7 to 9 DAPI bodies (Fig. 6I). *HTP-1(S325A)* germ lines also exhibit pachytene progression defect (Fig. 6D), reduced brood size (201.15 ± 9.9 versus 271.3 ± 5.54 in wild type, $P < 0.0001$), embryonic lethality (56.83 ± 1.95 versus 0 in wild type), and Him phenotype (5.04 ± 0.53% versus 0.06 ± 0.03% in wild type) (Fig. 6, F to H). Thus, *HTP-1(S325A)* is a loss-of-function allele, since complete loss of *htp-1* in null animals results in 94% embryonic lethality; of the 6% that survive, 24% present with Him phenotype (*41*). These data suggest that phosphorylation of HTP-1 at serine-325 activates its function. *HTP-1(S325E)* mutants did not display any significant defects for any of the parameters assayed (Fig. 6, E to H), which is consistent with HTP-1 phosphorylation being essential for HTP-1 function. These observations suggest that continuous phosphorylation of HTP-1(S325), as would be mimicked by replacement of serine by glutamic acid, does not have a gain-of-function–like effect likely because HTP-1 normally exists in a phosphorylated state in the oogenic germ cells.

To test whether HTP-1(S325) phosphorylation regulates oocyte number downstream to RAS/ERK signaling pathway, we assayed for oocyte number in *HTP-1(S325A)RAS(act)* and *ERK(loss);HTP-1(S325E)* double mutants (Fig. 7, A to G, and fig. S9, A to G). Notably, *HTP-1(S325A)* suppressed the *RAS(act)* mutant phenotype of increased oocytes and displayed a linear pattern of oocytes in 43.9% of the germ lines ($n = 41$) at 25°C (compare Fig. 7, D and E, and fig. S9,

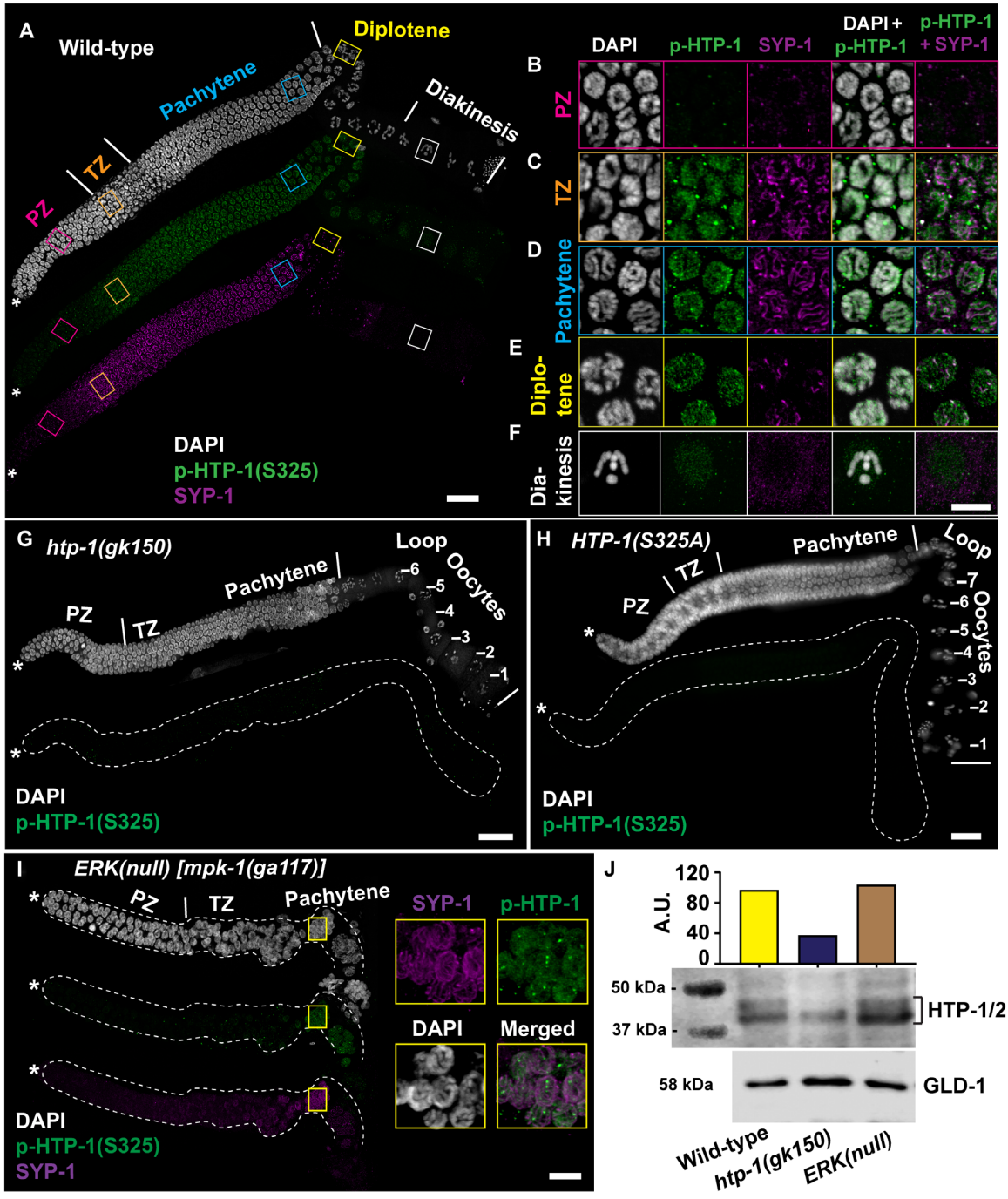

Fig. 5. HTP-1 is phosphorylated at S325 in vivo. The representative dissected germ lines are oriented with the DTC on the left (asterisks) of the photograph. (**A**) Immunolocalization of p-HTP-1(S325) (green), SYP-1 (to mark the central region protein of SC; magenta), and DAPI (DNA, white) in wild-type dissected germ line. (**B** to **F**) Magnified regions [corresponding to the boxes on (A)] of the indicated germ cell stages with individual and merged channels. p-HTP-1(S325) accumulates in nucleoplasm and chromatin in meiotic germ cells. (**G** to **H**) Representative dissected germ lines stained with p-HTP-1(S325) (green) and DAPI (white, DNA) from *htp-1(gk150)* deletion allele, and *HTP-1(S325A)* allele demonstrates lack of accumulation of p-HTP-1(S325). (**I**) Representative dissected germ lines from *mpk-1(ga117)* probed with anti–p-HTP-1(S325) (green) and anti–SYP-1 (magenta) display weak p-HTP-1(S325) accumulation in 10% of the germ lines. Yellow box highlights the regions in the inset. (**J**) Western blot analysis against anti–HTP-1/2 and GLD-1 proteins on wild-type, *htp-1(gk150)*, and *mpk-1(ga117)* animals reveals that HTP-1/2 total protein accumulation is not changed in *ERK(null)* worms compared to wild type. Anti–GLD-1 immunoblot was used as an internal loading control. Corresponding densitometric analyses for HTP-1/2 proteins are shown [top, in arbitrary units (A.U.)] as a ratio between HTP-1/2 and GLD-1 proteins and expressed as percentage. Experiments were repeated at least three times; $n \geq 10$ gonad arms per genotype were examined. Scale bars, 25 μm [for (A), (G), (H), and (I)] and 5 μm [for (B) to (F)].

D and E). Overall, the double-mutant germ lines exhibit significantly ($P < 0.0001$) lower oocyte number relative to *RAS(act)* single-mutant germ lines (Fig. 7H). Consistent with the suppression of *RAS(act)* by loss of HTP-1 phosphorylation, we observed that phosphomimetic *HTP-1(S325E)* rescued the lower oocyte number in *ERK(loss)* mutants at 25°C, restoring them to relative wild-type levels (Fig. 7, F and G, and fig. S9, F and G). Thus, we conclude that HTP-1 phosphorylation is necessary for regulating RAS/ERK pathway–dependent oocyte numbers. Because *HTP-1(S325E)* does not present with a *RAS(act)*-like phenotype as a single mutant, we hypothesize that RAS/ERK-mediated

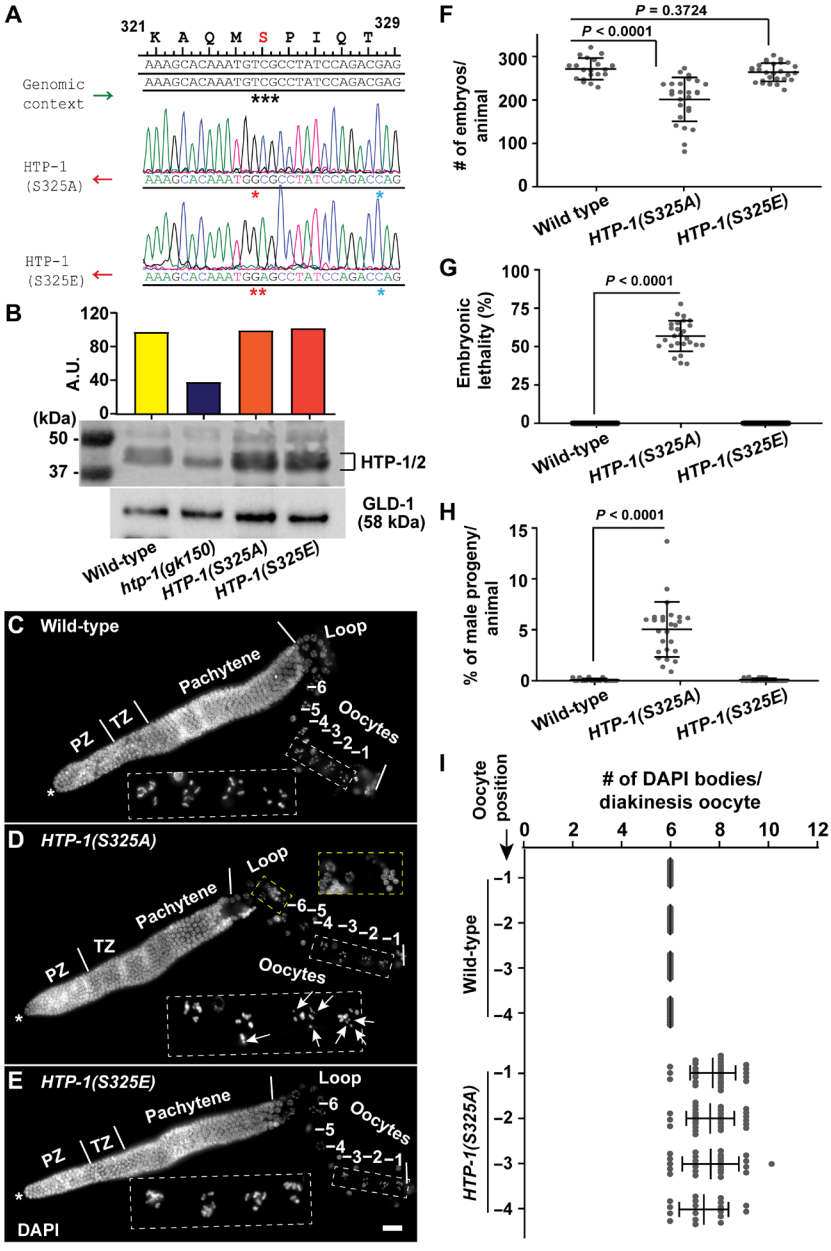

Fig. 6. HTP-1(S325) phosphorylation activates its function in vivo. (**A**) Sequence analysis of CRISPR-Cas9–edited animals. The figure displays the region surrounding the HTP-1(S325) locus (amino acids 321 to 329) from unphosphorylatable *HTP-1(S325A)* and phosphomimetic *HTP-1(S325E)* mutants. Red asterisks indicate changes to the DNA, blue asterisk indicates the silent mutation inserted to remove the Bsa I site, and black asterisks mark the S325 codon. (**B**) Western blot analysis against wild type and each of the *htp-1* mutant alleles using anti-HTP1/2 antibody. The upper HTP-1 band is absent from *htp-1(gk150)* and equally abundant in wild-type, *HTP-1(S325A)*, and *HTP-1(S325E)* lysates. Anti–GLD-1 immunoblot was used as an internal loading control. Corresponding densitometric analyses for HTP-1/2 proteins are shown (top, in arbitrary units) as a ratio between HTP-1/2 and GLD-1 proteins and expressed as percentage. (**C** to **E**) Dissected DAPI-stained germ lines of indicated genotypes displaying germline morphology. Inset is a magnified view of diakinesis oocytes −1 to −4 from each genotype. *HTP-1(S325A)* oocytes exhibit univalence (white arrows). Germ lines are oriented with the DTC on the left (asterisks). (**F** to **H**) Quantitative analysis of HTP-1 phospho-edited alleles for brood size, embryonic lethality, and Him phenotype. (**I**) Quantification of DAPI bodies (as a measure of univalence) in −1 to −4 diakinesis oocytes in *HTP-1(S325A)* compared to wild type. Data from the experiments showed in (F) to (I) were performed at 20°C and repeated three times; $n = 20$ to 30 per genotype were analyzed. Statistical significance was calculated by a nonparametric Mann-Whitney test, and *P* values are indicated between the groups compared. Error bars represent means ± SD. Scale bar, 25 μm.

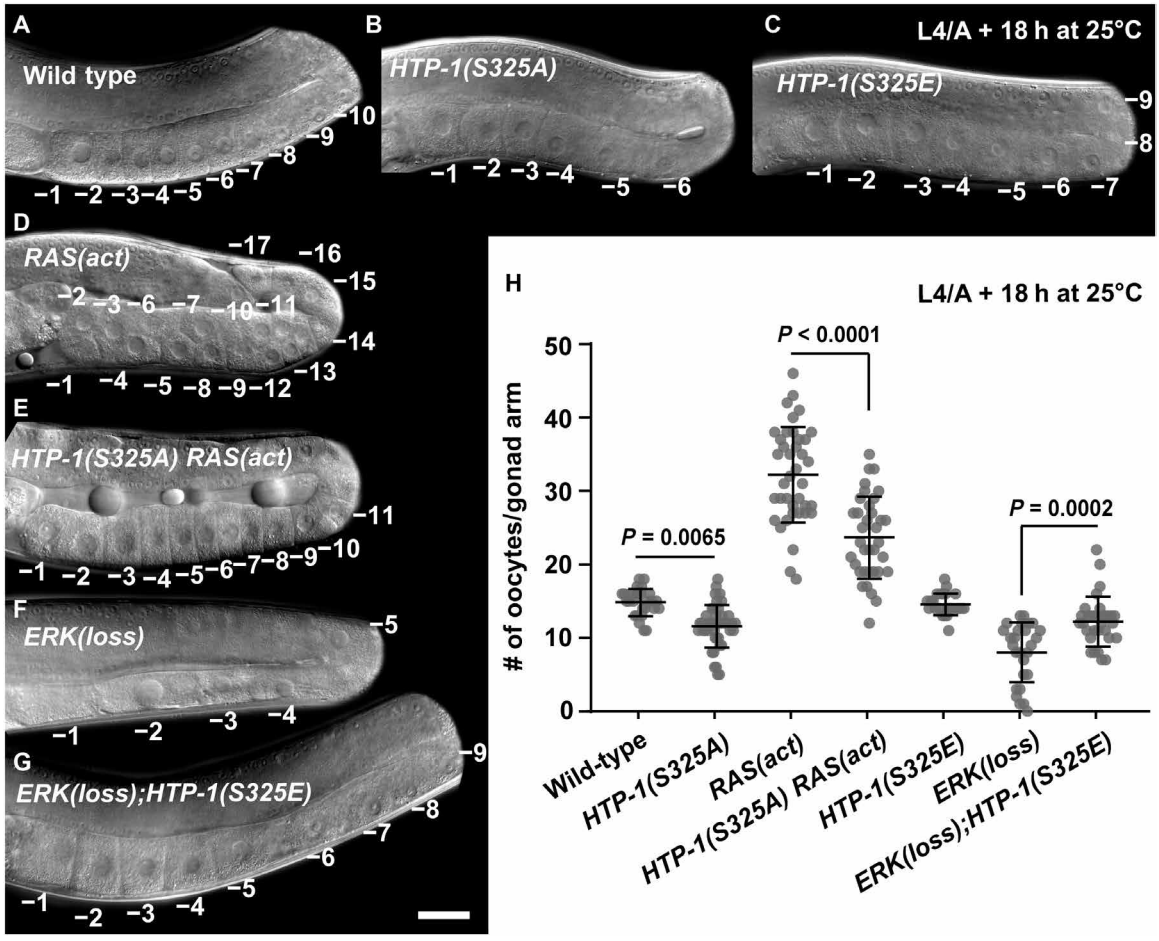

Fig. 7. RAS/ERK pathway regulates oocyte numbers through phosphorylation of HTP-1(S325). (**A** to **G**) Differential interference contrast (DIC) microscopy images of germ lines from indicated genotypes to visualize oocyte morphology. The loop region is on the right in the photographs and oocytes on the ventral side. Scale bar, 25 μm. (**H**) Scatter dot plot, with mean and SD, demonstrates quantification of oocyte number from the indicated genotypes. Oocytes were counted from dissected germ lines with anti–RME-2 and DAPI staining (Materials and Methods and fig. S9). Experiments were repeated three times, $n = 25$ to 44 per genotype. Statistical significance was calculated by a nonparametric Mann-Whitney test, and P values are indicated between the groups compared.

regulation of oocyte number is governed redundantly by HTP-1(S325) as well as through another substrate of ERK, such as HTP-3 or others, which currently remain unidentified.

HTP-1(S325) phosphorylation regulates synapsis extension, maintenance, and meiotic progression

To determine the cellular mechanism through which phosphorylated HTP-1 regulates oocyte number downstream to RAS/ERK signaling, we assayed for early meiotic progression via accumulation of p-SUN-1(S8) in HTP-1 phosphomutant backgrounds with *RAS(act)* and *ERK(loss)* mutants (fig. S10, A to G). We observed that *HTP-1(S325A)* displayed significantly ($P < 0.0001$) increased number of p-SUN-1(S8)–positive pachytene germ cell rows (30.89 ± 3.41) relative to *HTP-1(S325E)* or wild-type germ lines (22.67 ± 2.51 and 22.92 ± 1.97, respectively) (fig. S10, A, B, and H). This suggests that lack of HTP-1(S325) phosphorylation is sufficient to delay early meiotic progression. Next, to determine whether the altered rate of early meiotic progression in RAS/ERK mutants is reset upon loss or gain of HTP-1 phosphorylation, we assayed *HTP-1(S325A)RAS(act)* and *ERK(loss); HTP-1(S325E)* double mutants with p-SUN-1(S8). *HTP-1(S325A) RAS(act)* double-mutant germ lines display significantly ($P < 0.0001$) higher number of p-SUN-1(S8)–positive cell rows relative to *RAS(act)* single-mutant germ lines (20.00 ± 2.14 versus 16.08 ± 1.38, respectively) (fig. S10, C, D, and H). Conversely, *ERK(loss);HTP-1(S325E)* germ lines displayed a significantly ($P = 0.0139$) lower number of p-SUN-1(S8)–positive cell rows compared to *ERK(loss)* alone (fig. S10, F to H). Thus, we conclude that the HTP-1 phosphorylation is sufficient, in part, to rescue early meiotic progression defects in RAS/ERK mutants.

The expansion of p-SUN-1(S8) accumulation in mid-pachytene in *HTP-1(S325A)* is reminiscent of persistence of p-SUN-1(S8) in meiotic mutants that either display synapsis defects or have not satisfied the crossover assurance checkpoint. HTP-1 establishes early homolog alignment and prevents nonhomologous chromosome synapsis. Loss of HTP-1 results in severe asynapsis, a drastic reduction in meiotic crossover formation and activation of the crossover assurance checkpoint affecting meiotic progression (*41*, *42*). We hypothesize that phosphorylated HTP-1 regulates meiotic progression through regulating one of these components of meiosis I. To determine which step of the meiotic hierarchy was regulated by phosphorylation of HTP-1, we assayed for synapsis in *HTP-1(S325A)*

and *HTP-1(S325E)* mutant germ lines, which is an early step in meiosis I. Synapsis initiates in the TZ region at or near pairing centers, specialized regions required for homolog associations (*43*). Once initiated, the SC extends rapidly, largely irreversibly, to chromosome ends (*43*).

To examine whether HTP-1(S325) phosphorylation regulates SC extension and/or its maintenance, we took advantage of the spatiotemporal arrangement of germ cells in the *C. elegans* germ line. We assayed for synapsis in the early- and mid-pachytene chromosomes in *HTP-1(S325A)* germ lines using HIM-3 and SYP-1 immunostaining (Fig. 8, A to F). We observed partial or complete asynapsis of more than one chromosome in a given germ cell nucleus (Fig. 8, B and F), consistent with an increase in univalent chromosomes in diakinesis (Fig. 6I). Spatially, we observed asynapsed chromosomes in early pachytene in *HTP-1(S325A)* mutant germ lines (Fig. 8D) with the stretches of asynapsed chromosomes becoming significantly longer in the mid-pachytene region compared to early pachytene (Fig. 8B), suggesting that synapsis is neither formed nor maintained in *HTP-1(S325A)* mutant germ cells (Fig. 8F). We did not observe any asynapsis defects in the *HTP-1(S325E)* allele. These data together suggest that phosphorylation of HTP-1(S325) is essential for extension and/or maintenance of the SC.

To determine whether the asynapsis in the *HTP-1(S325A)* results in activation of the crossover assurance checkpoint, we assayed for meiotic DSBs since the presence of DSBs is a prerequisite for crossover designation and thus crossover assurance (*44*). RAD-51 functions to repair meiotic DSBs in preparation for homologous recombination (*4*). Because *C. elegans* lacks H2A.X (which marks DSBs) RAD-51 chromatin localized foci are widely used as a marker to assay for the level of DSB formation and to follow recombination dynamics. Defects in DSB formation should result in fewer RAD-51 foci, while defects in recombination should result in more RAD-51 foci. We thus assayed for RAD-51 foci in wild-type and *HTP-1(S325A)* germ lines. Consistent with previous observations in the field, we find that in wild-type germ lines, RAD-51 foci accumulate at their highest density in zone 3 (Fig. 9, A to H) with >85% of the germ cell nuclei harboring at least one RAD-51 focus (Fig. 9, C, E, F, and H). By zone 4, wild-type germ lines display fewer RAD-51 foci per germ cell nucleus with barely visible RAD-51 expression in zone 5 (Fig. 9, C and F). RAD-51 accumulation in *HTP-1(S325E)* germ lines follows a similar pattern to that of wild-type germ lines (Fig. 9H). Intriguingly, *HTP-1(S325A)* mirrors the dynamics of the wild-type germ line with the highest density of RAD-51 foci accumulating in zone 3, suggesting that lack of HTP-1 phosphorylation does not significantly impair formation or accumulation of DSBs (Fig. 9, B, D, and G). However, unlike wild-type germ lines where DSBs reduce in zone 4 and resolve in zone 5, we find that the DSBs in *HTP-1(S325A)* zone 4 are similar to those in zone 3, whereby the foci start to reduce in number by zone 5 and eventually resolve. These data suggest that there is an overall delay in DSB resolution upon lack of HTP-1 phosphorylation, likely due to the defects in synapsis formation and/or maintenance, which occurred in early-mid pachytene in *HTP-1(S325A)* mutant germ cells. Thus, we conclude that HTP-1 phosphorylation likely coordinates synapsis formation and maintenance to regulate meiotic progression.

To determine whether *ERK(loss)* mutants display any synapsis defects similar to *HTP-1(S325A)* animals and whether this defect was reversed by *HTP-1(S325E)* potentially underlying the cause of the rescue of low oocyte number, we assessed for synapsis in *RAS(act)* and *ERK(loss)* single mutants and in combination with HTP-1 phospho-alleles (Fig. 10, A to E, and fig. S11, A to H). At 25°C, *ERK(loss)* and *HTP-1(S325A)* single-mutant germ lines display 53.6% and 45.7% nuclei with asynapsed chromosomes in mid-pachytene stage, both here, and in subsequent paragraphs respectively, consistent with the role of ERK signaling in regulating SC dynamics. In contrast, wild-type, *RAS(act)*, and *HTP-1(S325E)* single-mutant germ lines display ~4% nuclei with asynapsed chromosomes in mid-pachytene stage (Fig. 10E). As predicted, *ERK(loss);HTP-1(S325E)* double mutants exhibit a reduction in number of mid-pachytene stage nuclei with asynapsed chromosomes from 53.6% in *ERK(loss)* alone to 25.2%, suggesting that *ERK(loss)*-mediated synapsis defects are due, in part, to the lack of HTP-1(S325) phosphorylation (Fig. 10E). Consistent with this observation, the lack of HTP-1(S325) phosphorylation led to an increase in asynapsis in mid-pachytene stage in *RAS(act)* mutant germ lines from 1.8 to 42.6%, resulting in a suppression of the increased oocyte number (Fig. 10E). Together, these data demonstrate that ERK-mediated HTP-1(S325) phosphorylation is necessary and sufficient for SC extension and/or maintenance to coordinate timely crossover formation, which, in turn, controls the rate of meiosis I progression and thus oocyte numbers.

DISCUSSION

"*.... cells acquire positional values in a coordinate system, which they interpret by developing particular ways to give rise to spatial patterns*" was proposed by Lewis Wolpert (*45*) in his groundbreaking work 51 years ago on positional information in pattern formation in development. This central concept proposes that cells acquire positional identities and use these identities to interpret their fate and give rise to patterns. Extrapolating this concept to the spatiotemporal organization of the meiotic germ cells in the context of a signal (ERK activation) that varies continuously along the distal-proximal axis of the tissue, we propose that activation of ERK in distal meiotic cells (early-pachytene), which normally do not receive this information at this position, results in the cells acquiring a more proximal (mid-pachytene) positional identity. The distal cells then interpret this information and proceed through events of meiosis I as if they were more proximal, resulting in a tissue that loses its stereotypical pattern of oocyte formation, number, and quality (Fig. 10). Thus, while the actual time that the cells spend in each spatial position may not change, the progression of meiosis I does, as interpreted by the cells in their individual positions along the coordinate system. Together, our data suggest that ERK activation provides the signal gradient in early-mid pachytene, which interprets and coordinates SC formation and/or maintenance with meiotic progression and formation of healthy oocytes and progeny (Fig. 10).

RAS/ERK signaling links environmental and metabolic cues to regulate cell numbers during tissue development across metazoans (*16*, *18*). In the *C. elegans* germ line, as in other organ systems in animals (*19*, *20*), RAS/ERK signaling regulates oocyte numbers: An increase in RAS signaling results in a sharp increase in oocyte number, and a decrease in ERK signaling causes a corresponding decrease in oocyte number (*11*, *17*). We show that in the germ line, RAS/ERK pathway does not regulate either proliferation or apoptosis to control oocyte numbers. At first glance, this is an unexpected result because of the prevailing models of RAS-mediated regulation of cell numbers (*19*, *20*, *46*). Our work goes on to show that the RAS/ERK signaling pathway regulates progression of meiosis I by phosphorylation

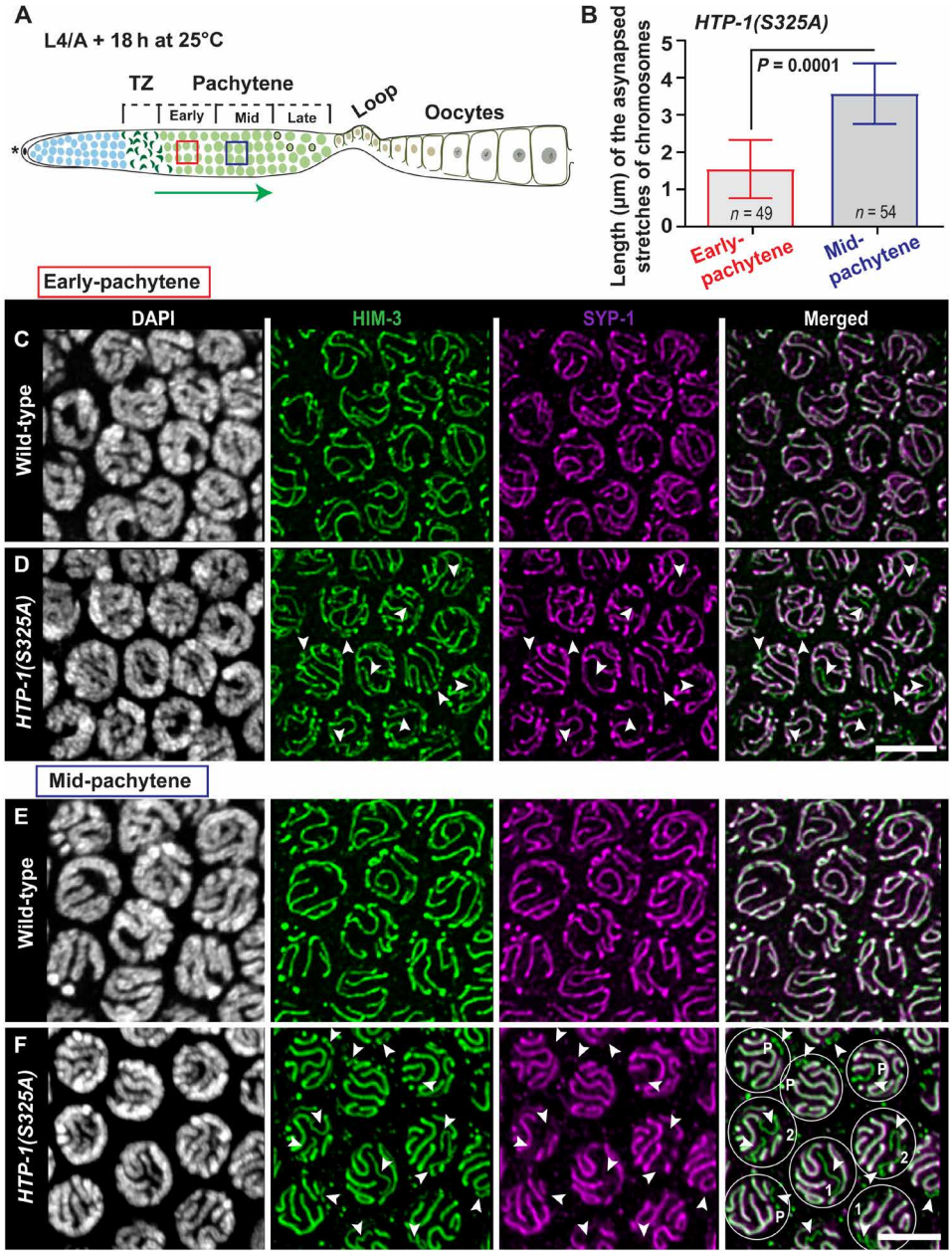

Fig. 8. HTP-1(S325) phosphorylation is necessary for synapsis extension and/or maintenance. (**A**) Schematic of an adult *C. elegans* hermaphroditic germ line. Red and blue boxes show the early- and mid-pachytene regions of the germ line, green arrow indicates the direction of meiotic progression. (**B**) Quantitation of the asynapsed chromosome lengths from HTP-1(S325A) using Imaris and ImageJ software (Materials and Methods). (**C** to **F**) Representative confocal images of germ cells from wild-type and *HTP-1(S325A)* mutants labeled with HIM-3 (axial element of SC, green), SYP-1 (central region of SC, magenta), and DAPI (DNA, white). Arrowheads indicate the stretches of chromosome lacking an SYP-1 label (asynapsed chromosomes). Note the presence of either partial (P) or completely asynaped chromosomes. When completely asynapsed, one (1) and two (2) asynapsed chromosomes in the mid-pachytene germ cells [(E), merged] are visible. Experiment was repeated three times; $n \geq 10$ gonad arms per genotype were examined. Scale bars, 5 µm.

of HORMA domain protein HTP-1, which, in turn, stabilizes the SC during meiosis I and allows meiotic progression (Fig. 10F). Lack of ERK signaling or lack of HTP-1 phosphorylation results in an inability of the SC to be properly extended or maintained, which effectively delays the chromosomal transition of cells from pachytene stage of meiotic prophase I to diplotene stage of oocytes. These data turn the light on a new mechanism of controlling cell numbers by signaling pathways, which are independent of canonical modes of regulation such as apoptosis and proliferation. Since this is the first report of such a regulation, given the conservation in RAS signaling across species, we propose that a similar mechanism may be responsible for regulating cell numbers by RAS in multiple contexts.

Previously, a central region protein, SYP-2, had been shown to be regulated by ERK signaling in *C. elegans* to mediate chromosome segregation (*36*); in our hands, SYP-2 was not labeled in vitro by ERK phosphotransfer assay. We surmise that this could be due to a

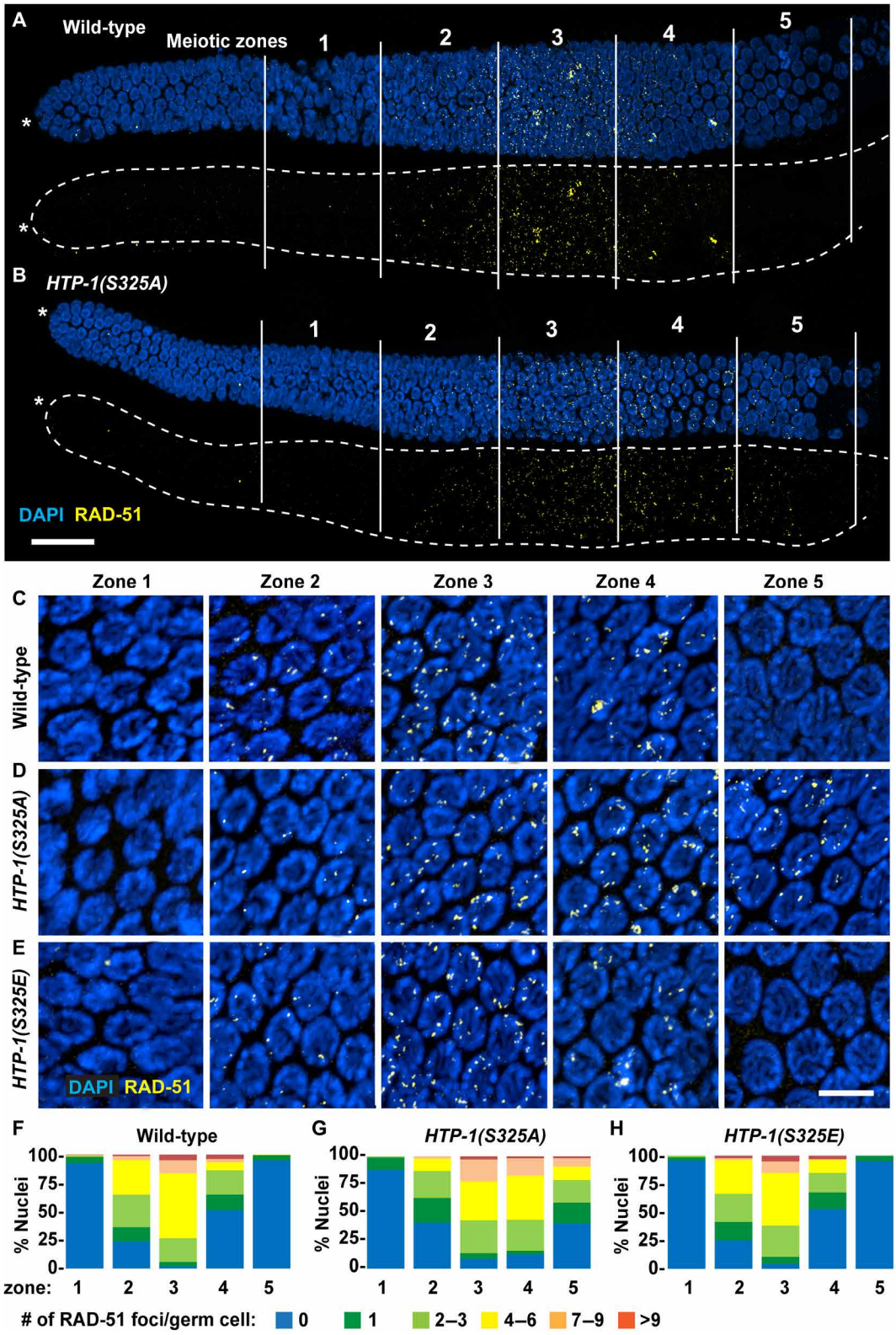

Fig. 9. Meiotic DNA DSBs persist in *HTP-1(S325A)* mutant germ lines. (**A** and **B**) Representative dissected germ lines from distal tip (left, asterisks) until the end of pachytene (right) from indicated genotypes probed with DAPI (DNA, blue) and RAD-51 antibody (to detect meiotic DSBs, yellow). White lines segment the germ line into distinct meiotic zones 1 to 5. (**C** to **E**) Magnified germ cells from each meiotic zone labeled with RAD-51 foci from the indicated genotypes. (**F** to **H**) Bar graphs with the quantification of RAD-51 foci in the germ cells from each meiotic zone [shown in (A) to (C)] of the indicated genotype displayed as percent RAD-51 foci. Experiment was repeated twice; $n > 150$ germ cells per zone per genotype were examined. Scale bars, 25 μm [for (A) and (B)] and 5 μm [for (C) to (E)].

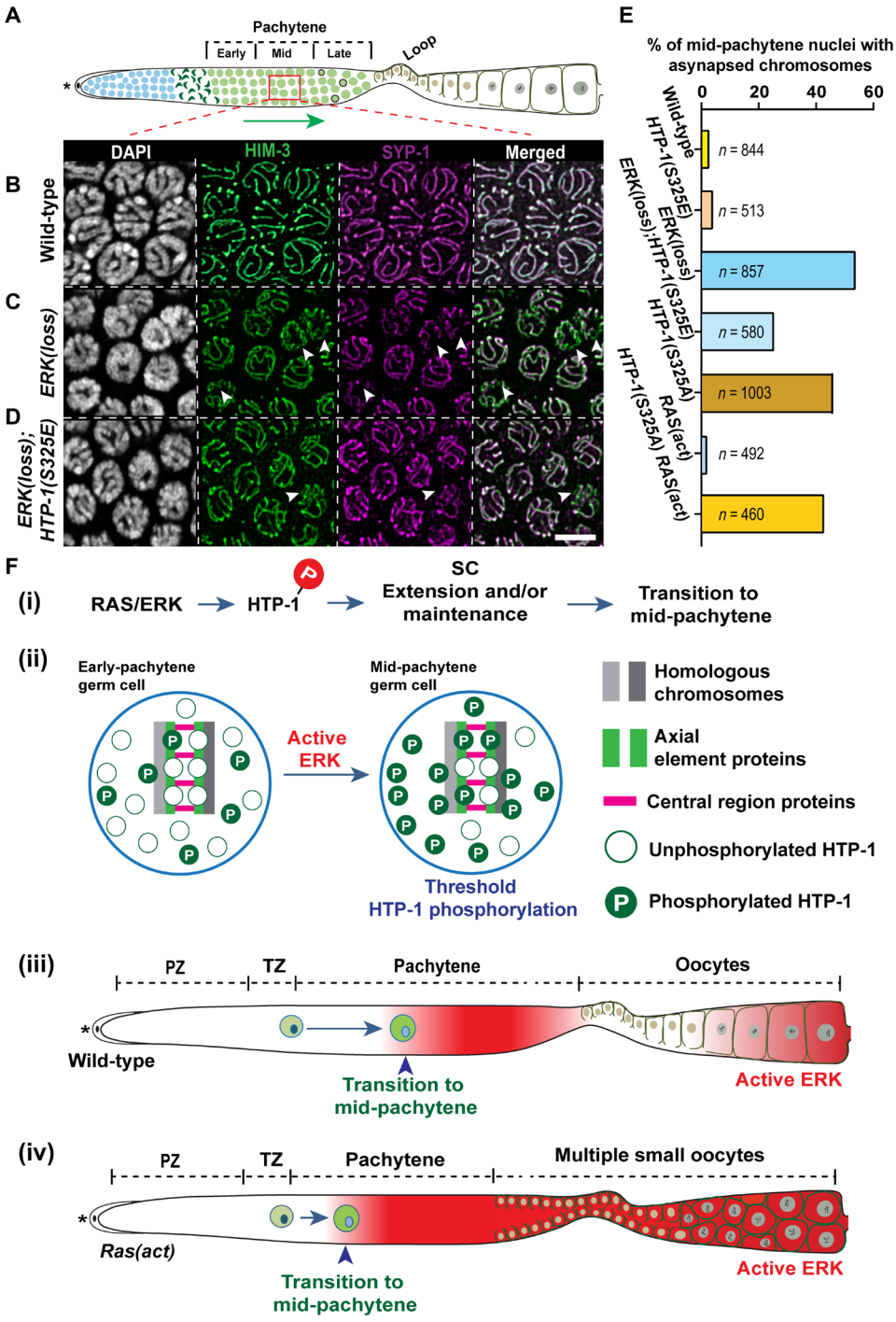

Fig. 10. HTP-1(S325) phosphorylation monitors the formation and/or maintenance of synapsis and regulates progression of meiosis I and oocyte production. (**A**) Schematic view of an adult *C. elegans* hermaphroditic germ line; red box shows the region (mid-pachytene) of the germ line displayed in the bottom panels, and green arrow indicates the direction for meiotic progression. (**B** to **D**) Representative confocal images of indicated genotypes probed with HIM-3 (axial element, green), SYP-1 (central element, magenta), and DAPI (DNA, white). Arrowheads indicate the stretches of chromosome lacking SYP-1 (asynapsed chromosomes). Loss of ERK activation results in increased asynapsis, which is reversed by restoration of HTP-1 phosphorylation. Scale bar, 5 μm. (**E**) Quantification of mid-pachytene germ cells with asynapsed chromosomes from germ lines of the indicated genotypes expressed in percentage. Total number of germ cells counted (*n*) in the mid-pachytene region/genotype is indicated on the bars. (**F**) Model presenting the cellular and molecular mechanism through which the RAS/ERK signaling pathway regulates oocyte number: (i) RAS/ERK signaling controls the progression of meiosis I in the early- and mid-pachytene regions by phosphorylating HTP-1 at S325. (ii) The threshold of ERK-dependent p-HTP-1 (S325) controls the transition of germ cells from early- to mid-pachytene stage. (iii and iv) Spatially early onset of ERK activation in *RAS(act)* mutant germ cells results in an increased threshold of HTP-1(S325) precociously causing distal pachytene stage cells to take on proximal identities, followed by early exit from pachytene stage germ cells to diplotene stage oocytes of the pachytene stage. Thus, spatial activation of ERK coordinates meiotic progression with oocyte formation.

difference in experimental setup. That axial components of the SC are phosphorylated by ERK signaling adds a new layer of regulation to the dynamic range of chromosome behaviors, in particular because the HORMA domain proteins form the base of the scaffold that builds and supports the SC (*4*, *6*, *7*, *47*). It is likely that phosphorylation-based scaffold formation allows for multiple heterotypic interactions between SC proteins that help stabilize the SC to allow for the various chromosome movements, which are essential for recombination and remodeling. Our data document a phosphosignaling cascade (RAS/ERK/HTP-1) in SC extension and/or maintenance. We propose that each of the phosphoprotein axial elements is necessary to initiate extension and stabilization of the SC and, in turn, control the progression of meiosis I. Thus, loss of even a single phosphorylation event such as in HTP-1(S325A) results in SCs that either do not extend or fail to maintain. In this case, the germ cells do not progress through pachytene as in wild type and are delayed, as evidenced by p-SUN-1(S8) accumulation pattern. In addition, in a background of increased RAS signaling, where all the substrates are likely to be phosphorylated, loss of one substrate phosphorylation [HTP-1(S325)] results in asynapsis and extension of meiotic DSBs, effectively reversing the phenotype of precocious meiotic progression (relative to wild type) and increased oocyte number. We also find that while phosphorylation of HTP-1 is necessary in SC dynamics, constitutive phosphorylation of HTP-1 is not sufficient to drive precocious meiotic progression. Thus, phosphomimetic HTP-1(S325E) does not by itself mimic increased RAS phenotype of multiple oocytes. It is likely that constitutive phosphorylation of HTP-3, or other currently unidentified substrate, function redundantly in vivo with HTP-1(S325) for this to occur. However, constitutive phosphorylation of HTP-1(S325E) is sufficient to rescue the ERK loss-of-function phenotype likely because in this context, all the ERK substrates are poorly phosphorylated and constitutive phosphorylation of one allows for partial stabilization of the SC and restores some of the SC phenotypes.

Together, we propose that the phosphorylation of HORMA domain proteins HTP-1 generates a phosphoproteome SC scaffold that allows for dynamic organization of the SC to coordinate the need of the germ line with the environmental conditions. Under nutrient-replete conditions, optimal RAS/ERK signaling results in normal progression of meiosis I, resulting in generation of healthy oocytes. However, in events of low nutrient levels or unfavorable environmental conditions, ERK signaling is low (*16*), resulting in lower phosphorylation of the HORMA domain protein that, in turn, slows down the extension and/or maintenance of SC, which effectively slows down the generation of oocytes. In this situation, oocytes would not be formed until the conditions return to normal, which will have a short-term impact on reproductive fitness; however, because the quality of the few oocytes formed upon return to favorable conditions will be high, the long-term impact on reproductive fitness would be minimal. In addition, because the progeny would be born from high quality oocytes under replete conditions, the chance of progeny survival would also be higher. This model directly links the regulation of chromosome behavior during early phases of meiosis I to dynamic control by environmental signaling and female reproductive fitness (Fig. 10F). Given the conservation of female meiosis I progression across species, we speculate that a similar signaling-based mechanism may be operative in mammalian females to regulate oocyte number and ovarian reserve.

MATERIALS AND METHODS

C. elegans maintenance

All strains (Table 1) were maintained at 20°C on plates made from standard nematode growth medium [NGM; NaCl (3 g/liter), Bacto peptone (2.5 g/liter), Bacto agar in distilled water (17 g/liter), with cholesterol (1 ml/liter) (5 mg/liter in ethanol), 1 M $CaCl_2$ (1 ml/liter), 1 M $MgSO_4$ (1 ml/liter), and 1 M potassium phosphate buffer (25 ml/liter, pH 6.0)]. OP50 *Escherichia coli* was used as the food source (Table 2) (*48*). The temperature-shift experiments were performed by placing L4/Adult molt animals from indicated genotypes at 25°C for 18 hours, unless otherwise noted. A parallel set of control experiments with the genotypes was conducted at 20°C each time.

Live imaging of worms

Five animals were mounted (each time) with 10 μl of 0.1 M levamisole in M9 on 2% agarose pads and imaged with Zeiss Axio Imager M2 equipped with an AxioCam MRm camera (Zeiss). All images were obtained using AxioVision software (Zeiss) as a montage of images at ×40.

Oocyte number counting

Oocyte numbers were counted by (i) live imaging using the membrane pH domain tagged with green fluorescent protein (GFP), to mark germ cell membranes (see Table 1 for the strains), and (ii) analysis of dissected and fixed oocytes labeled with RME (receptor mediated endocytosis)–2 (to mark oocytes) and mCherry::H2B (to mark chromosomal morphology) captured with *Z*-stacks (0.6 μm). Irrespective of method used, the datasets fall within the range of SD for that group and were reproducible within the replicates.

Germ cell nucleus counts and mitotic index

Germ cell counts and mitotic index were calculated as described previously (*49*). In brief, each germ cell nucleus was visualized by DAPI. PZ cells were defined as DAPI positive and HIM-3 negative. The number of germ cell nuclei (in PZ or entire germ line) was determined by a semiautomated method using a custom ImageJ Macro. The M-phase index was calculated as the number of p-histone H3–positive cells in the PZ divided by the total number of cells in the PZ multiplied by 100.

HU treatment

A stock of 850 mM HU was prepared in Milli-Q filtered water, and 300 μl was added to a 10-cm OP50-seeded standard NGM plate, followed by overnight incubation. Worms synchronized at 20°C until 6 hours past L4/adult molt stage were transferred to the HU-treated plates for 12, 18, or 24 hours and incubated at either 20° or 25°C. The animals were dissected, stained with anti–p-histone H3 (Ser^{10}) to assay proliferation and anti–RME-2 to assay oocyte number. Total germ cell number was counted manually from the acquired *Z*-stack (0.6 μm) images of the DAPI-stained gonad arms by the semiautomated method using a custom ImageJ Macro. Twelve hours of HU treatment was used for data analysis, since this treatment time displayed >~80% of germ lines with no proliferative cells. Eighteen hours of HU treatment coupled with the temperature shift also displayed no proliferative PZ cells and a similar phenotype as the 12-hour treatment; however, the longer treatment times led the *RAS(act)* oocytes to undergo endomitosis, which, in turn, leads to loss of membrane markers (fig. S3), causing errors in analysis. Thus, this time point was not used.

Table 1. *C. elegans* strains. The following *C. elegans* strains were used in this study.

Strain name [name used in this study]	Genotype
N2 [Wild type]	Wild type
BS3364	*mpk-1(ga111 rf)III = ERK(loss)* in the study
AUM1265	*let-60(ga89 gf)IV = RAS(act)* in the study
BS3675	*bcIs39 [lim-7p::ced-1::GFP + lin-15(+)]V*
AUM1265a	*mpk-1(ga111 rf) III; bcIs39 [lim-7p::ced-1::GFP + lin-15(+)]V*
MD771	*let-60(ga89 gf) IV; bcIs39 [lim-7p::ced-1::GFP + lin-15(+)]V*
MT1522	*ced-3(n717)IV*
AUM1273	*mpk-1(ga111 rf)III;ced-3(n717)IV*
AUM1034	*ltIs38 [(pAA1) pie-1p::GFP::PH(PLC1delta1) + unc-119(+)] III; ltIs37 [pie-1p::mCherry::his-58 (pAA64) + unc-119(+)]IV*
AUM1038	*mpk-1 (ga111 rf) ltIs38 [(pAA1) pie-1p::GFP::PH(PLC1delta1) + unc-119(+)] III; ltIs37 [pie-1p::mCherry::his-58 (pAA64) + unc-119(+)]IV*
AUM1032	*ltIs38 [(pAA1) pie-1p::GFP::PH(PLC1delta1) + unc-119(+)] III; let-60(ga89 gf) ltIs37 [pie-1p::mCherry::his-58 (pAA64) + unc-119(+)]IV*
AUM1606	*htp-1(viz62 [S325A])IV = HTP-1(S325A)* in the study
AUM1607	*htp-1(viz67 [S325E])IV = HTP-1(S325E)* in the study
AUM1564	*htp-1(viz76[S325A])let-60(ga89 gf) IV = HTP-1(S325A) RAS(act)* in the study
AUM1591a	*mpk-1(ga111)III; htp-1(viz67[S325E])IV = ERK(loss); HTP-1(S325E)* in the study
BS3830	*mpk-1(ga117) /qC1[dpy-19(e1259) glp-1(q339)qIs26]III. = ERK(null)* in the study
VC257	*htp-1(gk150)IV*
FX30203	*tmC25[unc-5(tmIs1241)]IV*

Table 2. Bacterial strains. The following bacterial strains were used in this study.

Bacterial strains		
E.coli : OP50	Caenorhabditis Genetics Center	OP50
E.coli : TOP10	Thermo Fisher Scientific, MA	Catalog no. C404003
E.coli : DH5a	Thermo Fisher Scientific, MA	Catalog no. 18265017
E.coli : BL21(DE3) pLysS	Millipore, CA	Catalog no. 69451-M
E.coli : BL21(DE3) pLysE	Sigma-Aldrich, MO	Catalog no. B9058

Apoptosis assay

Cell corpses were defined as CED-1::GFP–positive cells (see Table 1 for the strains). The animals were anesthetized, mounted, and visualized under an epifluorescence microscope. CED-1::GFP–marked germ cells were counted manually from the acquired *Z*-stack (0.6 μm) images of the gonad arms. CED-1 is a scavenger receptor. In the transgenic line used in this study, *lim-7* promoter drives CED-1::GFP in the gonadal sheath cells (*27*, *50*), enabling the visualization of germ cell engulfment by the somatic gonad.

Germline dissection, immunofluorescence staining, and microscopy

After each experiment, worms (n = 80 to 100) were dissected as described (*51*). Dissected worms were fixed in 3% formaldehyde with 100 mM K_2HPO_4 (pH 7.2) for 10 min at room temperature washed with phosphate-buffered saline (PBS) and 0.1% Tween 20 (PBST) and postfixed with 100% methanol (−20°C) for 1 hour [for di-phosphorylated (dp) ERK, GLD-1, RME-2, XND-1, p-SUN-1(S8), and p-HTP-1(S325) antibodies] or overnight (for HIM-3, p-histone H3, SYP-1, HTP-1/2, and RAD-51 antibodies). Fixed gonads, in batches, were washed with PBST and blocked with 30% normal goat serum for 1 hour at room temperature (for dpERK, GLD-1, RME-2, XND-1, and p-SUN-1 antibodies) or 3 hours [HIM-3, p-histone H3, SYP-1, p-HTP-1(S325), HTP-1/2, and RAD-51 antibodies] before incubation with the desired primary antibody as described (*51*). For p-histone H3 (1:400), HIM-3 (1:800), and SYP-1 (1:200) staining, germ lines were incubated in primary antibody for 4 hours at room temperature. dpERK (1:400)–, GLD-1 (1:200)–, RME-2 (1:600)–, XND-1 (1:800)–, p-SUN-1(S8) (1:800)–, p-HTP-1(S325) (1:400)–, HTP-1/2 (1:400)–, and RAD-51 (1:2000)–treated germ lines were incubated in primary antibody overnight at 4°C and processed as described (*51*) (see the antibodies in Table 3). Images were acquired either with Zeiss Axio Imager M2 equipped with an AxioCam MRm camera (Zeiss) or with an inverted laser scanning confocal microscope (Zeiss LSM 800). All images were obtained as a montage at ×40 or ×63 with overlapping cell boundaries. Images for a given antibody staining were taken with identical exposures and processed with ImageJ software. The montages were then assembled in Adobe Photoshop CS3 and processed identically.

RNAi of *him-3* and *spo-11*

The RNAi clones for *him-3* and *spo-11* were obtained from the Vidal library (Vidal ORFeome Library) and sequenced to verify integrity. Clones were grown overnight on LB agar plates containing ampicillin (100 μg/ml) at 37°C. Single colonies were inoculated in LB liquid cultures containing ampicillin (100 μg/ml) and grown to necessary densities as described previously (*17*). The cultures were seeded onto the standard NGM agar plates supplemented with 1 mM isopropyl β-D-1-thiogalactopyranoside and ampicillin (100 μg/ml). RNAi experiments were performed as described earlier (*17*) in the wild-type and in *RAS(act)* worms at the permissive temperature (20°C). Three to four adult (24 hours past L4) worms were placed on the RNAi plates overnight for embryo lay. The mothers were removed the next morning. The embryos were grown on the plate until adulthood. Sixty to 70 L4/A molt stage worms were placed on

Table 3. Antibodies and other reagents. Antibodies, bacterial strains, and other chemicals used in this study are presented in a tabular form below. HRP, horseradish peroxidase.

Reagent or resource	Source	Identifier
Antibodies		
Phospho-histone H3 (Ser^{10})	Millipore, CA	05-806
HIM-3	Sdix, DE	5347.00.02
RME-2	B. Grant	(*54*)
dp-ERK (anti-MAPKYT)	Sigma-Aldrich, MO	M8159
GLD-1	T. Schedl	(*31*)
XND-1	J. Yanowitz	(*33*)
p-SUN-1 (S8)	V. Jantsch	(*32*)
SYP-1	A. Villeneuve	(*55*)
p-HTP-1(S325)	This study	
RAD-51	Sdix	2948.00.02
HTP-1/2	A. Dernburg	
Anti-poly-Histidine	Sigma-Aldrich, MO	H1029
Goat–anti-mouse Alexa Fluor 555	Invitrogen, CA	A-21422
Goat–anti-rabbit Alexa Fluor 488	Invitrogen, CA	A-11008
Goat–anti-guinea pig Alexa Fluor 555	Invitrogen, CA	A-11076
Goat–anti-guinea pig Cy5	Abcam, MA	ab102372
Anti-rabbit HRP	MilliporeSigma, MO	NA934
Anti-mouse HRP	Thermo Fisher Scientific, MA	1858413

fresh RNAi plates and either transferred to 25°C or maintained at 20°C for 18 hours for analysis.

Expression of recombinant axial element and central region proteins

Recombinant fusion proteins were generated by cloning full-length complementary DNAs for each of the axial element and central region components into pTrcHis Topo (Invitrogen, catalog no. K4410-01) bacterial expression vectors (Table 2) to generate N-terminally 6× His-tagged proteins as described (*17*). HTP-1 unphosphorylatable mutant proteins were generated through site-directed mutagenesis as described (*17*). Positive clones were verified by sequencing. Recombinant proteins were expressed in BL21(DE3) (Sigma-Aldrich) cells at 37°C by using 1 mM isopropyl β-D-1-thiogalactopyranoside (dioxane free) for 3 to 4 hours. Proteins were purified by using Ni–nitrilotriacetic acid agarose. The expression of proteins was confirmed by Western blot analysis with anti-His (Sigma-Aldrich, no. H1029). LIN-1 used in these experiments is a glutathione *S*-transferase–tagged protein (*52*).

In vitro kinase assay by using activated murine ERK2

Purified ERK2 kinase was purchased from New England Biolabs (catalog no. P6080S), and in vitro kinase reactions with the purified recombinant proteins were carried out as described (*17*). After phosphotransfer, the proteins were resolved on to a 4 to 20% SDS–polyacrylamide gel electrophoresis (Bio-Rad, catalog no. 5671094). The gel was then dried at 60°C under vacuum for 1 hour and exposed to the autoradiographic film (Sigma-Aldrich, catalog no. 864 6770) for 4 or 16 hours at −80°C. The film was developed using the Kodak X-OMAT 2000A processor machine.

CRSIPR-Cas9–meditated generation of unphosphorylatable and phosphomimetic HTP-1 alleles

The unphosphorylatable and phosphomimetic alleles at the endogenous locus of *htp-1* were generated with a co–CRISPR-Cas9 method as described (*40*). To generate the unphosphorylatable HTP-1 mutant, serine-325 was mutated to alanine. To generate a phosphomimetic mutant, serine-325 was mutated to glutamic acid. Two potential CRISPR cut sites flanking the serine-325 were identified, and the corresponding Crispr(cr)RNAs were ordered from Dharmacon:

GTTGACGACATTACTGTTAC, 1026 base pairs (bp) downstream of the start codon

ACAACACGAAGAGGUGCTGA, 1134 bp downstream of the start codon

The repair template sequence contained the desired edit and 35 nucleotide homology arms outside of the crRNA recognition site. Five silent mutations were added on the crRNA recognition sites to prevent re-cutting by Cas9 after editing. One silent mutation was added to take out the Bsa I restriction site. This resulted in the following single-stranded oligo donors (ssODN) with the missense mutations (in bold) and the silent mutations (in lowercase):

For HTP-1(S325A):

GATCAAGGAGGAAACGAGACTTCTCCGGTtGAcGAcATtACTGTTAcTTTATTAGTTTTTTACATATAAACAAAAAATTTAAAATTGTAGGAGTCTCTCGAGAAAGCACAAATG**G**CGCCTATCCAGACcAGACCAACaACaCGaAGAGGtGCtGATGGCAGCAAAACC

For HTP-1(S325E): GATCAAGGAGGAAACGAGACTTCTCCGGTtGAcGAcATtACTGTTAcTTTATTAGTTTTTTACATATAAACAAAAAATTTAAAATTGTAGGAGTCTCTCGAGAAAGCACAAATG**GA**GCCTATCCAGACcAGACCAACaACaCGaAGAGGtGCtGATGGCAGCAAAACC

An injection mix was made as described (*40*) and injected into N2 young adult animals. Roller F_1s were screened for the mutation by polymerase chain reaction (PCR) digestion using the following primers: ACG GCT AAT TTT CGA TTG GAG T (forward) and ACT AAG GAT ACA ATA ATG GAG CAG AA (reverse), followed by overnight Bsa I restriction enzyme digestion (1 IU/10 μl PCR product). The PCR results in a wild-type product of 650 bp, which, upon restriction digestion, yields two bands at 450 and 200 bp. Because the phospho-edit removes the Bsa I cut site, heterozygous edited worms display three bands at 650, 450, and 200 bp, and homozygous edited worms display a single band at 650 bp upon restriction digestion. Four independent founders with accurate sequence were followed up for analysis. Homozygous worms from each founder line were outcrossed four times with the N2 wild-type strain, balanced (on *tmC25 [unc-5(tm1241 Venus]*) and used in the experiments. All founders displayed identical phenotypes.

htp-1 and *let-60* are on chromosome IV, and ~3.5 map units apart. Thus, the double-mutant *HTP-1(S325A)let-60(ga89)IV* double mutants were generated by CRISPR editing of *let-60(ga89)* as described above. Four founder lines were obtained with the desired sequence and analyzed after four backcrosses.

mpk-1(ga111)III; *HTP-1(S325E)IV* double mutants were generated by crossing *mpk-1(ga111)* with the *HTP-1(S325E)* animals. The progeny was screened using the strategy stated above for HTP-1(S325E), followed by sequence verification of the *mpk-1(ga111)* locus and *htp-1*(S325E) edit.

Brood size analysis, embryonic lethality, and % Him phenotype

Ten early L4 hermaphroditic worms of the indicated genotypes were placed individually on plates. A total of three replicates were performed. Every 24 hours, the parent worm was moved to a fresh plate, and the total number of embryos was counted on the original plate. This process was repeated over 5 to 7 days until the worms stopped producing progeny. The total number of embryos (across the entire lay period) was added up for each animal and then averaged between replicates. Embryonic lethality was calculated as the total number of larvae or adults on the plates subtracted from the number of embryos as follows [(number of embryos − number of adults)/numbers of embryos] × 100. The "Him" phenotype was calculated as the percentage of F_1 male progeny produced by one P0 hermaphrodite as follows: [total number of F_1 males/total numbers of adults] × 100.

Phospho-specific HTP-1(S325) antibody generation and purification

To generate p-HTP-1(S325) phospho-specific antibody, phosphopeptide (AQM[pS]PIQ) was synthesized and high-performance liquid chromatography fractionated (CPC Scientific Inc., CA). A C-terminal Cys-Lys-Lys-Lys was added to facilitate maleimide-based conjugation of peptides to KLH for immunization and to bovine serum albumin for purification of the antibodies. Sera were generated from immunized rabbits by Yenzym Antibodies, LLC (CA). Affinity purification of the phosphopeptide antibody and specificity testing were done as described (*17*, *38*, *53*). The phosphopeptide antibody was tested in vivo from specificity to HTP-1 and phosphorylated HTP-1, using *htp-1(gk150)* deletion allele and HTP-1(S325A), *htp-1(viz62)* phospho-null mutant germ lines.

Western blot analysis of whole worm protein extract

Whole worm protein extract and Western blot analysis was performed as described (*31*). Briefly, adult worms from respective genotypes were hand-picked (~200 for each genotype), washed in M-9 buffer, and boiled for 2 min with 2× loading dye at 95°C. The *mpk-1 (ga117)* germ lines are smaller than wild type because they are arrested in early-mid pachytene. Thus, 2.5× as many worms (~500 worms) as wild type were used per lane to obtain an equivalent amount of protein. Western blot analysis was performed as described (*31*) with anti–HTP-1/2 (1:600) and anti–GLD-1 (1:800), followed by anti-rabbit secondary antibody (1:2000). GLD-1 protein levels were used to normalize the germline content from each genotype. For quantification of band intensity, Western blots were converted to gray-scale images in Adobe Photoshop. The intensity of the bands was calculated using Fiji (ImageJ). The intensity of the GLD-1 bands was used as the control to calculate the relative amount of HTP-1/2 and expressed in percentage as arbitrary units (A.U.).

Confocal microscopy and analysis of asynapsed germ cells

Immunofluorescence images for p-HTP-1(S325), HIM-3, and SYP-1 (asynapsis assays) were captured with an inverted laser scanning confocal microscope (Zeiss LSM 800). Images were acquired as *Z*-stacks (0.19 μm) and deconvolved using the AutoQuant X3 deconvolution software. Images were processed in Fiji (ImageJ) for quantitation. The top five stacks of DAPI, HIM-3, and SYP-1 were projected maximally and overlaid in Adobe Photoshop to display the figures presented. Asynapsed germ cells from the mid-pachytene region were counted manually by assessment of colocalization between HIM-3 and SYP-1; cells where SYP-1 did not accumulate and colocalize with HIM-3 were termed "asynapsed." Percentage of these cells was calculated as follows: asynapsed germ cells/total number of germ cells × 100. The length of the asynapsed chromosome stretch was assayed using the Filaments module in the Imaris imaging software (Imaris x64, version 9.5.1; Oxford Instrument). The Filaments module was used to trace the asynaped stretch of the chromosome (with loss of SYP-1 staining), upon a DAPI channel "mask," which highlighted only the chromosomes. The data were measured over multiple *Z*-stacks, allowing for a measure along the three-dimensional configuration of the chromosome.

Quantification of RAD-51 foci

Immunofluorescence images for RAD-51 staining were captured with an inverted laser scanning confocal microscope (Zeiss LSM 800) in *Z*-stacks (0.19 μm) and processed in Fiji (ImageJ) for quantitation. The top five *Z*-stacks of DAPI and RAD-51 channels were projected maximally and overlaid in Adobe Photoshop. Quantitation of the foci was done manually; only nuclei that were completely contained within the image stack were scored. The germ line was divided into five consecutive zones from TZ until the end of pachytene. Occasional atypical nuclei with condensed, bright DAPI signals (apoptotic bodies) were excluded (mostly present in zones 4 and 5) from analysis. For each genotype, at least 150 nuclei per zone were calculated from five different germ lines.

Statistical analysis

Statistical analysis of data was done using GraphPad Prism 7.0 software. All datasets were checked for normal distribution using Wilk-Shaphiro test. In most experiments, the datasets did not follow a normal distribution pattern. Thus, *P* values were derived using the nonparametric Mann-Whitney *U* test. *P* values lower than 0.05 were considered statistically significant. Data graphs were plotted in GraphPad Prism using the scatter dot plots or bar graph displaying the SD from the mean value. *P* values are noted by brackets that indicate the groups being compared, and *n* values for each experiment are denoted in the corresponding figure legend.

SUPPLEMENTARY MATERIALS

Supplementary material for this article is available at http://advances.sciencemag.org/cgi/content/full/6/44/eabc5580/DC1

View/request a protocol for this paper from *Bio-protocol*.

REFERENCES AND NOTES

1. B. Ata, A. Seyhan, E. Seli, Diminished ovarian reserve versus ovarian aging: Overlaps and differences. *Curr. Opin. Obstet. Gynecol.* **31**, 139–147 (2019).
2. E. Pelosi, A. Forabosco, D. Schlessinger, Genetics of the ovarian reserve. *Front. Genet.* **6**, 308 (2015).
3. M. De Felici, F. G. Klinger, D. Farini, M. L. Scaldaferri, S. Iona, M. Lobascio, Establishment of oocyte population in the fetal ovary: Primordial germ cell proliferation and oocyte programmed cell death. *Reprod. Biomed. Online* **10**, 182–191 (2005).
4. K. J. Hillers, V. Jantsch, E. Martinez-Perez, J. L. Yanowitz, Meiosis. *WormBook* **2017**, 1–43 (2017).

5. D. Zickler, N. Kleckner, Recombination, pairing, and synapsis of homologs during meiosis. *Cold Spring Harb. Perspect. Biol.* **7**, a016626 (2015).
6. S. L. Page, R. S. Hawley, The genetics and molecular biology of the synaptonemal complex. *Annu. Rev. Cell Dev. Biol.* **20**, 525–558 (2004).
7. C. K. Cahoon, R. S. Hawley, Regulating the construction and demolition of the synaptonemal complex. *Nat. Struct. Mol. Biol.* **23**, 369–377 (2016).
8. B. J. Lesch, D. C. Page, Genetics of germ cell development. *Nat. Rev. Genet.* **13**, 781–794 (2012).
9. M. A. Handel, J. C. Schimenti, Genetics of mammalian meiosis: Regulation, dynamics and impact on fertility. *Nat. Rev. Genet.* **11**, 124–136 (2010).
10. N. Bhalla, A. F. Dernburg, A conserved checkpoint monitors meiotic chromosome synapsis in Caenorhabditis elegans. *Science* **310**, 1683–1686 (2005).
11. M.-H. Lee, M. Ohmachi, S. Arur, S. Nayak, R. Francis, D. Church, E. Lambie, T. Schedl, Multiple functions and dynamic activation of MPK-1 extracellular signal-regulated kinase signaling in Caenorhabditis elegans germline development. *Genetics* **177**, 2039–2062 (2007).
12. H.-Y. Fan, Q.-Y. Sun, Involvement of mitogen-activated protein kinase cascade during oocyte maturation and fertilization in mammals. *Biol. Reprod.* **70**, 535–547 (2004).
13. M.-H. Verlhac, H. de Pennart, B. Maro, M. H. Cobb, H. J. Clarke, MAP kinase becomes stably activated at metaphase and is associated with microtubule-organizing centers during meiotic maturation of mouse oocytes. *Dev. Biol.* **158**, 330–340 (1993).
14. H.-Y. Fan, Z. Liu, M. Shimada, E. Sterneck, P. F. Johnson, S. M. Hedrick, J. S. Richards, MAPK3/1 (ERK1/2) in ovarian granulosa cells are essential for female fertility. *Science* **324**, 938–941 (2009).
15. D. L. Church, K.-L. Guan, E. J. Lambie, Three genes of the MAP kinase cascade, mek-2, mpk-1/sur-1 and let-60 ras, are required for meiotic cell cycle progression in Caenorhabditis elegans. *Development* **121**, 2525–2535 (1995).
16. A. L. Lopez III, J. Chen, H.-J. Joo, M. Drake, M. Shidate, C. Kseib, S. Arur, DAF-2 and ERK couple nutrient availability to meiotic progression during *Caenorhabditis elegans* oogenesis. *Dev. Cell* **27**, 227–240 (2013).
17. S. Arur, M. Ohmachi, S. Nayak, M. Hayes, A. Miranda, A. Hay, A. Golden, T. Schedl, Multiple ERK substrates execute single biological processes in *Caenorhabditis elegans* germ-line development. *Proc. Natl. Acad. Sci. U.S.A.* **106**, 4776–4781 (2009).
18. S. T. Eblen, *Advances in Cancer Research* (Elsevier, 2018), vol. 138, pp. 99–142.
19. F. Chang, L. S. Steelman, J. G. Shelton, J. T. Lee, P. M. Navolanic, W. L. Blalock, R. Franklin, J. McCubrey, Regulation of cell cycle progression and apoptosis by the Ras/Raf/MEK/ERK pathway (Review). *Int. J. Oncol.* **22**, 469–480 (2003).
20. W. Zhang, H. T. Liu, MAPK signal pathways in the regulation of cell proliferation in mammalian cells. *Cell Res.* **12**, 9–18 (2002).
21. D. M. Eisenmann, S. K. Kim, Mechanism of activation of the *Caenorhabditis elegans* ras homologue *let-60* by a novel, temperature-sensitive, gain-of-function mutation. *Genetics* **146**, 553–565 (1997).
22. M. R. Lackner, S. K. Kim, Genetic analysis of the *Caenorhabditis elegans* MAP kinase gene *mpk-1*. *Genetics* **150**, 103–117 (1998).
23. J. Liang, S. Balachandra, S. Ngo, L. E. O'Brien, Feedback regulation of steady-state epithelial turnover and organ size. *Nature* **548**, 588–591 (2017).
24. J. Pellettieri, A. S. Alvarado, Cell turnover and adult tissue homeostasis: From humans to planarians. *Annu. Rev. Genet.* **41**, 83–105 (2007).
25. H. D. Ryoo, T. Gorenc, H. Steller, Apoptotic cells can induce compensatory cell proliferation through the JNK and the Wingless signaling pathways. *Dev. Cell* **7**, 491–501 (2004).
26. I. H. Krakoff, N. C. Brown, P. Reichard, Inhibition of ribonucleoside diphosphate reductase by hydroxyurea. *Cancer Res.* **28**, 1559–1565 (1968).
27. B. Lant, W. B. Derry, Fluorescent visualization of germline apoptosis in living *Caenorhabditis elegans*. *Cold Spring Harb. Protoc.* **2014**, 420–427 (2014).
28. Z. Zhou, E. Hartwieg, H. R. Horvitz, CED-1 is a transmembrane receptor that mediates cell corpse engulfment in *C. elegans*. *Cell* **104**, 43–56 (2001).
29. E. A. Kritikou, S. Milstein, P.-O. Vidalain, G. Lettre, E. Bogan, K. Doukoumetzidis, P. Gray, T. G. Chappell, M. Vidal, M. O. Hengartner, *C. elegans* GLA-3 is a novel component of the MAP kinase MPK-1 signaling pathway required for germ cell survival. *Genes Dev.* **20**, 2279–2292 (2006).
30. T. L. Gumienny, E. Lambie, E. Hartwieg, H. R. Horvitz, M. O. Hengartner, Genetic control of programmed cell death in the Caenorhabditis elegans hermaphrodite germline. *Development* **126**, 1011–1022 (1999).
31. A. R. Jones, R. Francis, T. Schedl, GLD-1, a cytoplasmic protein essential for oocyte differentiation, shows stage- and sex-specific expression during *Caenorhabditis elegans* germline development. *Dev. Biol.* **180**, 165–183 (1996).
32. A. Woglar, A. Daryabeigi, A. Adamo, C. Habacher, T. Machacek, A. la Volpe, V. Jantsch, Matefin/SUN-1 phosphorylation is part of a surveillance mechanism to coordinate chromosome synapsis and recombination with meiotic progression and chromosome movement. *PLOS Genet.* **9**, e1003335 (2013).
33. C. R. Wagner, L. Kuervers, D. L. Baillie, J. L. Yanowitz, *xnd-1* regulates the global recombination landscape in *Caenorhabditis elegans*. *Nature* **467**, 839–843 (2010).
34. A. F. Dernburg, K. McDonald, G. Moulder, R. Barstead, M. Dresser, A. M. Villeneuve, Meiotic recombination in *C. elegans* initiates by a conserved mechanism and is dispensable for homologous chromosome synapsis. *Cell* **94**, 387–398 (1998).
35. M. C. Zetka, I. Kawasaki, S. Strome, F. Müller, Synapsis and chiasma formation in *Caenorhabditis elegans* require HIM-3, a meiotic chromosome core component that functions in chromosome segregation. *Genes Dev.* **13**, 2258–2270 (1999).
36. S. Nadarajan, F. Mohideen, Y. B. Tzur, N. Ferrandiz, O. Crawley, A. Montoya, P. Faull, A. P. Snijders, P. R. Cutillas, A. Jambhekar, M. D. Blower, E. Martinez-Perez, J. W. Harper, M. P. Colaiacovo, The MAP kinase pathway coordinates crossover designation with disassembly of synaptonemal complex proteins during meiosis. *eLife* **5**, e12039 (2016).
37. N. Ferrandiz, C. Barroso, O. Telecan, N. Shao, H.-M. Kim, S. Testori, P. Faull, P. Cutillas, A. P. Snijders, M. P. Colaiácovo, E. Martinez-Perez, Spatiotemporal regulation of Aurora B recruitment ensures release of cohesion during *C. elegans* oocyte meiosis. *Nat. Commun.* **9**, 834 (2018).
38. S. Arur, M. Ohmachi, M. Berkseth, S. Nayak, D. Hansen, D. Zarkower, T. Schedl, MPK-1 ERK controls membrane organization in *C. elegans* oogenesis via a sex-determination module. *Dev. Cell* **20**, 677–688 (2011).
39. M. Camps, A. Nichols, S. Arkinstall, Dual specificity phosphatases: A gene family for control of MAP kinase function. *FASEB J.* **14**, 6–16 (2000).
40. A. Paix, A. Folkmann, G. Seydoux, Precision genome editing using CRISPR-Cas9 and linear repair templates in *C. elegans*. *Methods* **121–122**, 86–93 (2017).
41. F. Couteau, M. Zetka, HTP-1 coordinates synaptonemal complex assembly with homolog alignment during meiosis in *C. elegans*. *Genes Dev.* **19**, 2744–2756 (2005).
42. E. Martinez-Perez, A. M. Villeneuve, HTP-1-dependent constraints coordinate homolog pairing and synapsis and promote chiasma formation during *C. elegans* meiosis. *Genes Dev.* **19**, 2727–2743 (2005).
43. O. Rog, A. F. Dernburg, Direct visualization reveals kinetics of meiotic chromosome synapsis. *Cell Rep.* **10**, 1639–1645 (2015).
44. Z. Yu, Y. Kim, A. F. Dernburg, *Seminars in Cell & Developmental Biology* (Elsevier, 2016), vol. 54, pp. 106–116.
45. L. Wolpert, Positional information and patterning revisited. *J. Theor. Biol.* **269**, 359–365 (2011).
46. P. J. Roberts, C. J. Der, Targeting the Raf-MEK-ERK mitogen-activated protein kinase cascade for the treatment of cancer. *Oncogene* **26**, 3291–3310 (2007).
47. S. Köhler, M. Wojcik, K. Xu, A. F. Dernburg, Superresolution microscopy reveals the three-dimensional organization of meiotic chromosome axes in intact *Caenorhabditis elegans* tissue. *Proc. Natl. Acad. Sci. U.S.A.* **114**, E4734–E4743 (2017).
48. S. Brenner, The genetics of *Caenorhabditis elegans*. *Genetics* **77**, 71–94 (1974).
49. T. Furuta, H.-J. Joo, K. A. Trimmer, S.-Y. Chen, S. Arur, GSK-3 promotes S-phase entry and progression in *C. elegans* germline stem cells to maintain tissue output. *Development* **145**, dev161042 (2018).
50. R. Voutev, R. Keating, E. J. A. Hubbard, L. G. Vallier, Characterization of the *Caenorhabditis elegans* Islet LIM-homeodomain ortholog, *lim-7*. *FEBS Lett.* **583**, 456–464 (2009).
51. A. L. Gervaise, S. Arur, Spatial and temporal analysis of active ERK in the *C. elegans* germline. *J. Vis. Exp.* **2016**, e54901 (2016).
52. D. Jacobs, D. Glossip, H. Xing, A. J. Muslin, K. Kornfeld, Multiple docking sites on substrate proteins form a modular system that mediates recognition by ERK MAP kinase. *Genes Dev.* **13**, 163–175 (1999).
53. M. Drake, T. Furuta, K. M. Suen, G. Gonzalez, B. Liu, A. Kalia, J. E. Ladbury, A. Z. Fire, J. B. Skeath, S. Arur, A requirement for ERK-dependent Dicer phosphorylation in coordinating oocyte-to-embryo transition in C. elegans. *Dev. Cell* **31**, 614–628 (2014).
54. B. Grant, D. Hirsh, Receptor-mediated endocytosis in the *Caenorhabditis elegans* oocyte. *Mol. Biol. Cell* **10**, 4311–4326 (1999).
55. A. Woglar, A. M. Villeneuve, Dynamic architecture of DNA repair complexes and the synaptonemal complex at sites of meiotic recombination. *Cell* **173**, 1678–1691.e16 (2018).

Acknowledgments: We thank V. Jantsch, J. Yanowitz, and A. Dernburg for providing the p-SUN-1(S8), XND-1 and HTP-1/2 antibodies, respectively. We thank R. Roberts and colleagues at NEB for the supply of the active murine ERK2 enzyme. We thank members of the Arur Lab for critical discussions during the course of the study. We thank M. Galko and A. Kalia for critical comments on the manuscript. **Funding:** The Arur Lab is funded through NIGMS98200. D.D. is funded through Odyssey Postdoctoral Fellowship (supported by the Kimberly-Clark Foundation), MD Anderson Cancer Center. S.A. is an Andrew Sabin Family Foundation Fellow. Some strains were provided by the CGC, which is funded by NIH Office of Research

Infrastructure Programs (P40 OD010440). **Author contributions:** D.D. designed the study, conducted the experiments, interpreted data, and wrote the manuscript. S.-Y.C. conducted experiments and interpreted data. S.A. designed the study, interpreted data, and wrote the manuscript. **Competing interests:** The authors declare that they have no competing interests. **Data and materials availability:** All data needed to evaluate the conclusions of this paper are present in Figs. 1 to 10 and figs. S1 to S11. Additional data related to this paper may be requested from the authors.

Submitted 30 April 2020
Accepted 18 September 2020
Published 30 October 2020
10.1126/sciadv.abc5580

Citation: D. Das, S.-Y. Chen, S. Arur, ERK phosphorylates chromosomal axis component HORMA domain protein HTP-1 to regulate oocyte numbers. *Sci. Adv.* **6**, eabc5580 (2020).